Oceanologia (2021) 63, 194—213

Available online at www.sciencedirect.com

ScienceDirect

journal homepage: www.journals.elsevier.com/oceanologia

ORIGINAL RESEARCH ARTICLE

WAVEWATCH-III source terms evaluation for optimizing hurricane wave modeling: A case study of Hurricane Ivan

Mehdi Yaghoobi Kalourazi[a], **Seyed Mostafa Siadatmousavi**[a,*], **Abbas Yeganeh-Bakhtiary**[a], **Felix Jose**[b]

[a] *School of Civil Engineering, Iran University of Science and Technology, Narmak, Tehran, Iran*
[b] *Department of Marine & Earth Sciences, Florida Gulf Coast University, Fort Myers, FL, USA*

Received 19 August 2020; accepted 14 December 2020
Available online 26 December 2020

KEYWORDS
Third generation wave model;
Hurricane Ivan;
Whitecapping dissipation;
Swell dissipation;
Gulf of Mexico

Abstract Simulating hurricane-generated waves is a challenging task due to rapidly fluctuating wind speed and direction, simultaneous presence of swells propagating out of the previous location of the hurricane and following/opposing waves on either side of the hurricane track, and dissipation in wind speed radially from the center of the hurricane. Bulk wave parameters have been investigated using the source term packages ST3, ST4 and ST6 implemented in the WAVEWATCH-III model to determine the most appropriate formulation for simulating hurricane-generated waves in the Gulf of Mexico. Based on the comparisons between model results and in situ observations during the passage of Hurricane Ivan (2004), it is shown that ST3 is not as successful as other formulations for hurricane wave modeling. Calibrated ST6 variant, T12, has shown to be the best formulation for simulating bulk wave parameters at points within the range of hurricane wind forcing; however, for the area beyond, and also during fair weather conditions, calibrated ST4 formulation, T471-Ex4, is recommended. Although T471-EX4 and T12 packages outperformed other cases, they overestimated waves propagating in the oblique and

* Corresponding author at: School of Civil Engineering, Iran University of Science and Technology, Narmak, Tehran, Iran.
E-mail address: siadatmousavi@iust.ac.ir (S.M. Siadatmousavi).
Peer review under the responsibility of the Institute of Oceanology of the Polish Academy of Sciences.

Production and hosting by Elsevier

https://doi.org/10.1016/j.oceano.2020.12.001

opposing wind. Dependence of ST6 parameter a_0 on wind and wave direction is examined to improve the model performance.

1. Introduction

Third generation wave models (e.g. WAVEWATCH-III (Brenner et al., 2007), WAM (Hasselmann et al., 1988) and SWAN (Booij et al., 1999)) have been extensively used to study wind generated waves. Simulated bulk wave parameters using these models were in fair agreement when compared with observations during usual storm conditions (Allard et al., 2014; Beyramzade and Siadatmousavi, 2019; Fan et al., 2009; Kazeminezhad and Siadatmousavi, 2017; Moon et al., 2003; Phadke et al., 2003). The governing equation for such models is the conservation of the wave action which is also valid in the presence of surface current. It is written as follows:

$$\frac{\partial N}{\partial t} + \nabla . C_g N = \frac{S_{tot}}{\sigma} \quad (1)$$

where C_g is group velocity, $N(k,\theta) = \frac{F(k,\theta)}{\sigma}$ is action density spectrum, F is variance density spectrum, and σ is intrinsic frequency. The variance density spectrum is a function of wavenumber k, direction θ, time t and space x. The term S_{tot} represents all energy fluxes contributing to wind-wave evolution (Komen et al., 1996; Tolman et al., 2019; Young, 1999), and can be written as follows in deep water:

$$S_{in} + S_{nl} + S_{ds} = S_{tot} \quad (2)$$

where S_{in} is atmospheric input, S_{ds} is wave dissipation, and S_{nl} is nonlinear wave-wave interaction. Each of these terms can be further partitioned into smaller scale processes (Ardhuin et al., 2010; Babanin, 2011; Babanin and Westhuysen, 2008). In general, waves grow when wind speed is higher than the wave phase velocity. Mitsuyasu and Honda (1982) noted that the growth of wind-induced waves also relates to the wave steepness and the ratio of the wave phase velocity to the shear velocity. Belcher and Hunt (1993) showed that wave growth is maximum when $\frac{C_p}{u_*} \approx 12$, where C_P is phase velocity calculated using peak frequency f_p. In the case when $\frac{C_p}{u_*} > 15$, an opposing current is generated close to the surface, which inhibits wave growth. The drag force on waves increases the energy transfer from wind to wave. When wind and waves are in opposite directions, the wind does not transfer its energy to the wave. During such conditions, dissipation of wave energy depends on the wave steepness and wave age; such that increasing the wave steepness increases the energy dissipation (Hasselmann and Bösenberg 1991; Mitsuyasu and Yoshida, 2005; Peirson et al., 2003). The rate of wind-induced wave growth during following winds is estimated to be 6.9 to 12.6 times that of the attenuation rate during opposing wind (Young and Sobey, 1985). In addition, the dissipation is greater for high-frequency waves than low-frequency waves. Donelan (1999) estimated the negative growth rate as 2.5 times smaller compared to the positive wave growth in following wind.

The interaction between wind sea and swells and their growth and dissipation under varying wind effects have been studied earlier (Cheng and Mitsuyasu, 1992; Donelan and Pierson, 1987; Mitsuyasu and Maeda, 2002; Mizuno, 2003). This interaction results in the dissipation of wind sea, and the dissipation rate depends on the steepness of swell and the ratio of peak frequencies of swell and sea waves.

Based on the Australian Shallow Water Experiment, and *in situ* observations from the Lake George in Australia, Donelan et al. (2005) proposed a new approach for measuring microscale pressure-induced oscillations above surface waves and concluded that wave breaking plays an important role in the momentum exchange between wind and waves. Consistent wave growth was observed when $\frac{U_{10}}{C_p} = 5.1 \sim 7.1$, according to Donelan et al. (2006). They concluded that the rate of wave growth depends on wave steepness, which makes the input term a nonlinear function of the wave spectrum. Moreover, full air-flow separation occurred for strong winds, in which the airflow detached from the crests and reattached on the windward face, leaving a separation zone over the leeward face and the troughs. As a result, a reduction in the wind input source function was required, compared to intermediate wind conditions. Babanin et al. (2007) proposed that energy transfer from wind to waves could be parameterized using the sum of a nonbreaking input term and an additional term to include enhanced energy transfer to breaking waves.

The dissipation term includes wave-breaking, swell attenuation and negative input under opposing wind conditions. Negative wind input is considered as a negative growth rate in the wind input term (Donelan et al., 2006). The wave-breaking dissipation term included two mechanisms; the first one is an inherent breaking dissipation, which occurs at or below the spectral peak frequency and the second mechanism is a cumulative dissipative effect which accounts for dissipation of short waves caused by breaking of longer waves (Babanin and Young, 2005; Young and Babanin, 2006). Babanin (2009) evaluated and further calibrated the above-mentioned formulations. Zieger et al. (2011) implemented these new wind input and dissipation source terms in WAVEWATCH-III (hereafter WW3) and validated against buoy measurements for wind sea-dominated conditions. Rogers et al. (2012) implemented similar formulations developed by Babanin et al. (2010) in SWAN model. Swell dissipation is based on turbulent kinetic energy dissipation (Babanin, 2011). For waves below a critical steepness threshold, wave-breaking and white-capping dissipation are inactive, and swell dissipation is the main dissipation mechanism. Zieger et al. (2015) and Babanin (2011) also parameterized swell dissipation using wave generated turbulence (Ardhuin et al., 2009; Babanin, 2006; Babanin and Chalikov, 2012).

Various source term packages have been implemented in WW3 including: WAM3 known as ST1 (Komen and Hasselmann, 1984; Snyder et al., 1981), ST2 (Tolman and Chalikov, 1996), WAM4+ known as ST3 (Bidlot et al., 2007; Janssen, 1991), ST4 (Ardhuin et al., 2009; Ardhuin et al., 2010; Rascle and Ardhuin, 2013) and ST6 (Babanin and Young, 2005; Donelan et al., 2006; Rogers et al., 2012; Young and Babanin, 2006). A comparison study between ST6, ST2 and T471 (An alternative of ST4) showed that wave height estimated by ST6 is slightly larger than waves estimated by others packages due to its stronger growth rates (Zieger et al., 2015). It also produced a broader directional distribution in wave spectrum at the peak frequency, particularly when employed in combination with Discrete Interaction Approximation (DIA) for S_{nl}. Bi et al. (2015) reported that ST6 slightly better estimate swell dissipation. They showed that ST2 (ST6) overestimated (underestimated) wave energy in tropical and subtropical environments, and ST4 resulted in the best agreement with NDBC-buoy data in the Pacific Ocean. Christakos et al. (2020) investigated the performance of different formulations of the SWAN model in narrow fetch geometries and showed the overestimation of wave height by ST6. Kalantzi et al. (2009) showed none of ST1 and ST2 was able to appropriately simulate waves in the presence of swells. Applying WW3 for Northern Indian Ocean, Umesh and Behera (2020) concluded that ST4 outperformed other formulations for simulating the wave height.

Although WW3 is known to produce bulk wave parameters during hurricane conditions (Hanson et al., 2009; Jiang et al., 2010; Ortíz and Mercado, 2008; Padilla-Hernandez et al., 2004), performance of different packages is not similar. Liu et al. (2017) compared performances of ST2, ST3, ST4 and ST6 against measurements for Hurricane Ivan (2004). They found that ST2 was the least accurate formulation while ST4 outperformed other formulations in simulating wave height and wave period. Chao et al. (2005) have simulated waves during Hurricanes Lili (2002) and Isidore (2002). They specified that reduced drag coefficient, C_d, was required to avoid overestimation of wave height during extreme events as suggested by Powell et al. (2003) and Donelan et al. (2004). Zhao et al. (2011) implemented reduced C_d in the model and reported better agreement with in situ observations.

Mentaschi et al. (2015) simulated wave height and period using ST4 during severe weather conditions over seventeen case studies in the northern Tyrrhenian Sea and off the Mediterranean Spanish coast. The model overestimated highest wave heights during storm events but underestimated wave height at fair weather conditions.

High quality wind is required to have successful wave simulation (e.g. Siadatmousavi et al., 2015; Siadatmousavi et al., 2011). Long-term reanalysis wind data such as the National Centers for Environmental Prediction (NCEP), the European Centre for Medium-Range Weather Forecasts (ECMWF), and the Cross-Calibrated Multi-Platform (CCMP) might be used for wave simulations (Brenner et al., 2007; Cavaleri and Sclavo, 2006; Mazaheri et al., 2013; Moeini et al., 2012; Signell et al., 2005). To avoid wave height underestimation close to the hurricane eye, those datasets might be blended with H*wind (e.g. Siadatmousavi et al., 2011) or to be modified using data assimilation (e.g. Lakshmi H Kantha, 2000).

Among all factors affecting the simulation results, selecting a suitable source packages in the wave model is one of the key decisions given its non-linear relationship with hurricane forcing conditions. In this study, hurricane-induced waves in the Gulf of Mexico were simulated using WW3 during Hurricane Ivan (2004). NCEP and ECMWF wind datasets were evaluated to select the most suitable wind data during the study period. Performance different packages were evaluated by comparing model results with NDBC buoys as well as satellite altimetry data. The parameters controlling the wave growth as well as opposing wind interaction with waves during hurricane passages are fine-tuned in each package. Unlike earlier studies (e.g. Liu et al., 2017), skill assessment for all aforementioned packages were used after calibration.

2. Wind input and dissipation source terms of WW3

Several packages for wind input and dissipation terms are available in WW3 version 6.07 as explained in the following section.

2.1. WAM4+ package (ECWAM)

The wind–wave interaction source terms of WAM4 (hereafter ST3) are based on the wave growth theory proposed by Miles (1957) and modified by Janssen (1982). The wind input source term is defined as follows:

$$S_{in}(k,\theta) = \frac{\rho_a}{\rho_w}\frac{\beta_{max}}{\kappa^2}e^Z Z^4\left(\frac{u_*}{C}\right)\cos^{p_{in}}(\theta_w-\theta_u)\,\sigma N(k,\theta) + S_{out}(k,\theta) \tag{3}$$

$$Z = \log(kZ_1) + \frac{\kappa}{\left[\cos(\theta_w-\theta_u)\left(\frac{u_*}{C}+z_\alpha\right)\right]} \tag{4}$$

$$Z_1 = \alpha_0\frac{\tau}{\sqrt{1-\frac{\tau_w}{\tau}}} \tag{5}$$

$$U_{10} = \frac{u_*}{\kappa}\log\left(\frac{Z_u}{Z_1}\right) \tag{6}$$

where ρ_a and ρ_w are the air and water densities; β_{max} is a non-dimensional growth parameter; C is wave phase velocity; κ is von Karman's constant; u_* is friction velocity; σ is angular frequency and p_{in} is a constant controlling the directional distribution of S_{in}; θ_u is wind direction; z_u is the height at which the wind is specified and z_α is a wave age tuning parameter. Wave-supported stress τ_w is calculated in the model based on the high frequency tail of the spectrum. Several sets of values for these parameters are proposed in the manual. The last term in Eq. (3) is the swell feedback on wind input term, and it is calculated according to Janssen (2004) as follows:

$$S_{out}(k,\theta) = 2s_1\kappa\frac{\rho_a}{\rho_w}\left(\frac{u_*}{C}\right)^2\left[\cos(\theta_w-\theta_u) - \frac{\kappa C}{u_*\log(kz_0)}\right] \tag{7}$$

where s_1 varies from 0 to 1 to control this phenomenon. The general form of the WAM4 dissipation term is as follows:

$$S_{ds}(k,\theta)^{WAM} = C_{ds}\bar{\alpha}^2\bar{\sigma}\left[\delta_1\frac{k}{\bar{k}} + \delta_2\left(\frac{k}{\bar{k}}\right)^2\right]N(k,\theta) \quad (8)$$

where C_{ds} is a non-dimensional constant, and δ_1 and δ_2 are weight parameters, and $\bar{k}$ and $\bar{\sigma}$ are mean frequency and mean wave number.

2.2. Ardhuin et al. (2010) package

Ardhuin et al. (2010) proposed a package for wind input and dissipation (hereafter ST4 package) in which a positive part of the wind input is taken from ST3, with an ad hoc reduction of u_* to balance a saturation-based dissipation of waves. By reducing the wind input at high frequencies, the drag coefficient C_d reduces for high winds. The swell feedback on wind input is also included according to Ardhuin et al. (2009). A weighted combination of wave dissipation in viscous and turbulent boundary layers is employed for $S_{out}(k,\theta)$ (Rascle and Ardhuin, 2013). The dissipation term S_{ds} is defined as the sum of three terms: (1) the saturation based term which combines an isotropic part and a direction-dependent part; (2) the cumulative breaking term $S_{bk,cu}$ which represents the effect of long waves on short waves; (3) the wave-turbulence interaction term S_{ds}^{turb} (Ardhuin and Jenkins, 2006; Teixeira and Belcher, 2002).

2.3. BYDRZ package

In BYDRZ package (hereafter ST6) the term describing the energy transfer from wind to waves has the following features: (1) full air-flow separation that leads to a relative reduction in wind input for conditions of strong winds and steep waves; (2) dependence of wave growth rate on wave steepness, which signifies the nonlinear behavior of the wind-input source function. Following Rogers et al. (2012), this source term can be written as follows:

$$S_{in} = \frac{\rho_a}{\rho_w}\sigma\gamma(k,\theta)N(k,\theta) \quad (9)$$

$$\gamma(k,\theta) = G\sqrt{B_n(k)}W(k,\theta) \quad (10)$$

$$B_n(k) = A(k)N(k)\sigma k^3 \quad (11)$$

$$G = 2.8 - \left[1 + \tanh(10\sqrt{B_n(k)}W(k,\theta) - 11\right] \quad (12)$$

The omni-directional action density $N(k)$ is obtained by integration over all directions, and $A(k)$ is defined such that $A^{-1}(k) = \int_0^{2\pi}[N(k,\theta)/N_{max}(k)]d\theta$, where $N_{max}(k) = max\{N(k,\theta)\}$, for all directions $\theta \in [0, 2\pi]$ (Babanin and Solov'yev, 1987). The growth rate in Eq. (12) is parameterized by Babanin (2006) as follows:

$$W_1(k,\theta) = max^2\left\{0, 28\frac{u_*}{C}\cos(\theta_u - \theta_w) - 1\right\} \quad (13)$$

$$W_2(k,\theta) = min^2\left\{0, 28\frac{u_*}{C}\cos(\theta_u - \theta_w) - 1\right\} \quad (14)$$

$$W(k,\theta) = W_1(k,\theta) - a_0W_2(k,\theta) \quad (15)$$

In fact, Eq. (13–15) are used to produce appropriate directional distribution for the growth rate by considering following and opposing wind fields. The relation between wind speed and friction velocity is $U_{10} = 28u_*$ (i.e., $Y = 28$) based on Snyder et al. (1981) and Komen and Hasselmann (1984). Rogers et al. (2014) and Liu et al. (2018) proposed employing $U_{10} = 32u_*$ to improve model skills in estimating tail level.

The dissipation in ST6 includes a threshold function (T_1) and the cumulative dissipation effect (T_2) such that:

$$S_{ds}(k,\theta) = [T_1(k,\theta) + T_2(k,\theta)]N(k,\theta) \quad (16)$$

Details on the formulations of T1 and T2 can be found elsewhere (e.g. Babanin, 2011; Babanin et al., 2007; Liu et al., 2018). The swell attenuation mechanism might be active even in the absence of wave breaking. Babanin (2011) parametrized this phenomenon based on the interaction of waves with oceanic turbulence as follows:

$$S_{swl}(k,\theta) = -\frac{2}{3}b_1\sigma\sqrt{B_n}N(k,\theta) \quad (17)$$

where b_1 is a non-dimensional coefficient.

3. Data and method

3.1. Wind data

Gridded wind data for the study area were extracted from the European Centre for Medium-Range Weather Forecasts (ECMWF) as well as National Centers for Environmental Prediction (NCEP) including the National Center for Atmospheric Research (NCAR) and The North American Regional Reanalysis (NARR). Due to different temporal and spatial resolution of these datasets, they were evaluated to find the most suitable data for wave simulations. The data from ECMWF/ERA5 dataset was obtained from a meteorological model with ~ 30 km spatial resolution and at one-hour interval. NCEP/NARR model with ~ 32 km resolution at 3-hour interval was the other available source used for evaluation. Wind data were extracted for the period September 12th – 17th, 2004 during which Hurricane Ivan traversed across the Gulf of Mexico. Datasets were compared with hourly metdata from NDBC buoys deployed in the Gulf of Mexico (see Figure 1a).

3.2. Bathymetry

Bathymetry data were downloaded from the National Geophysical Data Center (NGDC, available online at http://www.ngdc.noaa.gov/mgg/gdas/gd_designagrid.html). US Coastal Relief Model Grids and ETOPO1 1-minute Global Relief Grid were used to interpolate depth at computational vertices which were $\frac{1}{8}^\circ$ apart in both spatial directions.

3.3. Remote sensing data

Significant wave height data derived from satellite altimetry compilation is unique for model assessment due to its spatial coverage. Available satellite-derived wave height data from ERS2, ENVISAT, TOPEX, JASON1 and GFO satellites were downloaded from GlobWave dataset via ftp server of the French Research Institute for Exploitation

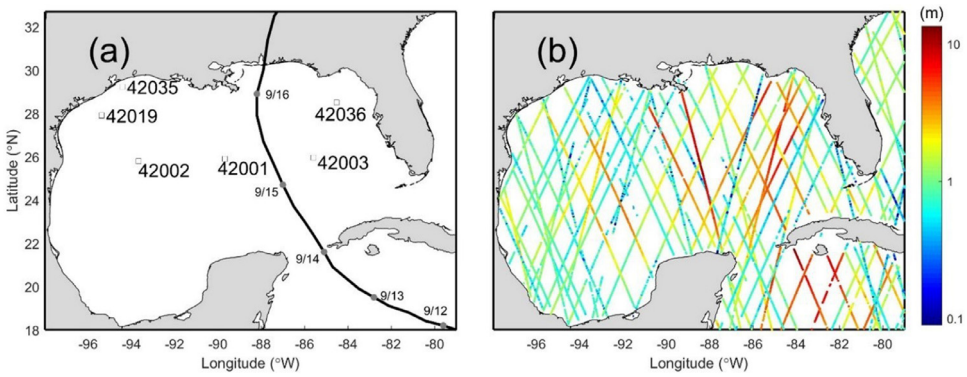

Figure 1 (a) Track of Hurricane Ivan that made landfall along the northern Gulf of Mexico in September 2004 and NDBC buoy locations used in this study; (b) tracks of satellites measuring wave height for the study period.

Table 1 Parameter values employed in the sensitivity analysis of the source term package.

WW3-ST4									WW3-ST3			
Parameter	T405	T471f	T471	T471-EX1	T471-EX2	T471-EX3	T471-EX4	Parameter	WAM4	BJA	BID	BJA-EX1
β	1.55	1.33	1.43	1.55	1.75	1.82	1.78	s_1	0	0	1	1
WW3-ST6												
Parameter	T1(V4.18)	T2	T3	T4	T5(V5.16)	T6(V6.07)	T7	T8	T9	T10	T11	T12
a_0	0.04	0.04	0.04	0.09	0.09	0.09	0.14	0.14	0.14	0.16	0.13	0.11
b_1	0.00025	0.0032	0.0041	0.00025	0.0032	0.0041	0.00025	0.0032	0.0041	0.0028	0.0044	0.0038

of the Sea (ftp://ftp.ifremer.fr/ifremer/cersat/products/swath/altimeters/waves/data). The satellite tracks and wave height data during Hurricane Ivan are presented in Figure 1b.

3.4. Hurricane Ivan

Hurricane Ivan, the strongest hurricane of 2004, resulted in widespread damage in the Caribbean and United States, and reached Category 5 strength on the Saffir-Simpson hurricane Scale. It was active during September 2nd—24th and passed across the Gulf of Mexico during September 13th—16th. The maximum wind velocity and minimum pressure at the center of the hurricane were reported as 165 kts and 910 hPa, respectively. Hurricane Ivan (2004) was selected for this study because the hurricane track passed almost through the midpoint of two NDBC buoys (42001 and 42002). The time period from the entry of the tropical storm into the Gulf of Mexico until its landfall along northern Gulf coast was selected for the wave simulations. The hurricane track and available buoys used for model validations (42001, 42002, 42003, 42019, 42039, and 42036) are shown in Figure 1a.

3.5. Numerical experiments with WW3

In order to quantitatively evaluate different source terms implemented in WW3, 23 test simulations were conducted for the selected source term packages ST3, ST4 and ST6. The parameter values selected for each test are summarized in Table 1. Tests T1 to T12 use ST6 package but with different values for coefficients a_0 and b_1 that control the interaction of opposing wind and swell dissipation. T405, T471, T471f are three sets of coefficients proposed in WW3 v6.07 for ST4 (Ardhuin et al., 2010; Rascle and Ardhuin, 2013). It is generally accepted that T471 works well at global scales with ECMWF winds; however, would cause a serious known problem of a negative bias when $H_s > 8$ m. Test T471f corresponds to a retuning of coefficients to force the model with CSFR wind reanalysis from NCEP/NCAR (Saha et al., 2010), and has almost no bias up to $H_s = 15$ m. The test T405 has relatively higher wave growth parameter β when compared to T471 and T471 f. The tests T471 $-$ $EX1$ to T471 $-$ $EX4$ are variants of the test T471 but with higher wave growth parameter β. The last configuration was to employ ST3 using BJA, WAM4, BID and BJA-EX1 values for coefficients among which BJA is the default setting. In all models, a regular 0.125° $\times$ 0.125° grid covering entire Gulf of Mexico (18—31.5° latitude, 98 —79W° longitude) was used. The frequency increment factor, the first frequency, the number of frequencies and the directions for all simulations were set as 1.1, 0.0425 Hz, 30 and 36, respectively. The bulk wave parameters such as wave height were calculated from hourly wave spectra using frequency range 0.0425—0.5 Hz to be consistent with NDBC buoys data.

3.6. Statistical indicators

In this study, Normalized Bias (NBI) and symmetrically normalized root mean square error (HH) indices were used for

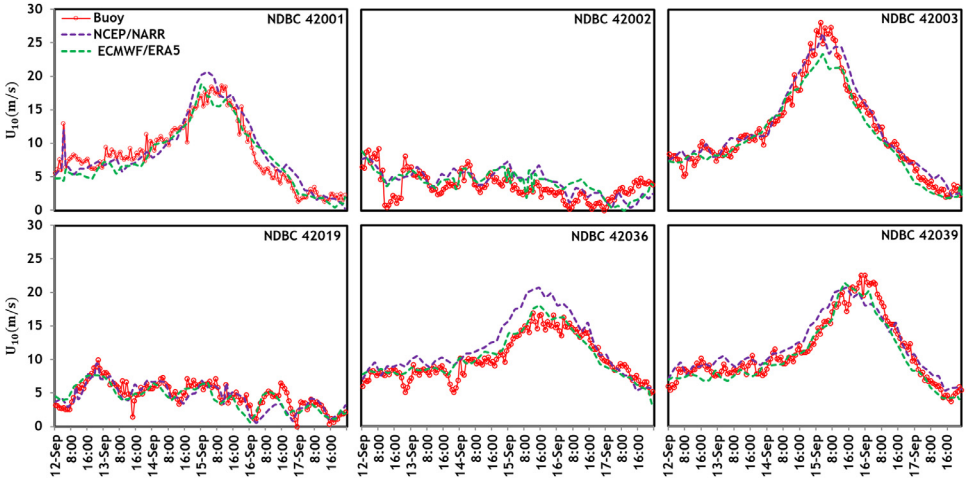

Figure 2 Wind speed data from the NCEP/ NARR and ECMWF/ERA5 plotted with observations at NDBC buoy locations.

model assessment. Their definitions are as follows:

$$\mathrm{NBI} = \frac{\sum(S_i - O_i)}{\sum O_i} \tag{18}$$

$$\mathrm{HH} = \sqrt{\frac{\sum (S_i - O_i)^2}{\sum S_i O_i}} \tag{19}$$

where S_i and O_i are simulation output and observations, respectively. The NBI index represents the mean error and the HH index proposed by Hanna and Heinold (1986) examines the scattering of simulated values. To compare the statistical data for wind and wave direction, normalized bias NBI_θ and normalized root mean square error NRMSE_θ can be used:

$$\mathrm{NBI}_\theta = \frac{\sum mod_{-\pi,\pi}(\theta_{Si} - \theta_{Oi})}{2\pi N} \tag{20}$$

$$\mathrm{NRMSE}_\theta = \frac{\sqrt{\sum [mod_{-\pi,\pi}(\theta_{Si} - \theta_{Oi})]^2 / N}}{2\pi} \tag{21}$$

where module operator ($mod_{-\pi,\pi}$) indicates that if $(\theta_{Si} - \theta_{Oi}) > \pi$, the 2π angle is subtracted from the angle differences, and if $(\theta_{Si} - \theta_{Oi}) < -\pi$, the 2π angle is added to the angle differences.

Another useful way to examine how close the model results are with respect to the observations is to use the Taylor diagram. The Taylor diagram schematically plots *RMSE*, standard deviation (σ) and correlation coefficient (ρ).

4. Results

4.1. Quantitative evaluation of wind data

A comparison between the ECMWF/ERA5 and NCEP/NARR wind data with measured wind velocity from NDBC buoys are shown in Figure 2. For better evaluation, the NBIAS and HH values for wind speeds are presented in Table 2. As shown in Figure 2, there is a good agreement between model and in situ data of wind speed from the NDBC buoys in the Gulf of Mexico. However, the NCEP/NARR data at the time of peak wind speed is slightly higher than the values measured at buoys. As inferred from Figure 2 and NBIAS values in Table 2, ECMWF/ERA5 underestimated the wind speed at relatively slow speeds (see 42001, 42003, 42019 and 42039 buoys), while NCEP/NARR model tends to overestimate the wind speed during high wind events, consistent with findings of Meissner et al. (2001). Based on HH and NBIAS values, there is a good agreement between all wind models and in situ observations (both for NDBC buoys data and satellite derived wind from the entire Gulf of Mexico); however, HH values confirm a slightly better quality for the NCEP/NARR model from different buoy sites; hence, this data product would be suitable for simulating the wave fields. As shown in Table 2, NCEP/NARR data are better than ERA5 in reproducing the wind direction also at different buoys.

To further improve the model wind input, data assimilation has been employed using the NDBC buoy data. It is an optimization process using statistical methods, based on which the model data are modified using a weight function. This function is based on the distances of model points from the observations. In this study, optimal interpolation method was used according to Hasselmann et al. (1997).

4.2. Model assessment for ST3

Four sets of parameters are used for ST3 assessments: WAM4, BJA, BID and BJA–EX1. The BJA and BJA–EX1 differ only in s_1 value. The coefficient s_1 is set to 1 when swell dissipation is considered and 0 otherwise. In Figure 3, the values of S_{in}, S_{ds} and S_{tot} at 42001 and 42003 buoys locations are presented for 08:00 on September 15th. When $f < f_p$, S_{in} is only negative for BID and BJA-EX1 at 42001, while S_{in} is positive in other tests at 42001 and 42003 buoys. Note that the buoys 42002, 42001 and 42019 are located on the left side of the hurricane track and the buoys 42003, 42036 and 42039 are located on the right side of hurricane track. The buoys on the left side of the Hurricane track experienced the young swell waves generated earlier. So, the interaction between wind sea and the swell caused a decrease in the wave height. NBIAS calculated for wave height is decreased for BJA-EX1 when compared to BJA at those buoys (see Table 3).

Table 2 Statistical comparison of wind speed and direction from NCEP/NARR and ECMWF/ERA5 with observations at buoy locations.

		NDBC-42001		NDBC-42002		NDBC-42003		NDBC-42019	
		ECMWF/ERA5	NCEP/NARR	ECMWF/ERA5	NCEP/NARR	ECMWF/ERA5	NCEP/NARR	ECMWF/ERA5	NCEP/NARR
U_{10}	**HH**	0.17	0.17	0.49	0.40	0.11	0.10	0.28	0.20
	NBIAS	-0.04	0.03	-0.04	0.09	-0.04	0.05	-0.12	-0.06
Dir	**NRMSE**$_\theta$	6.46	3.03	10.43	8.30	2.79	3.31	5.09	4.81
	NBIAS $_\theta$	0.70	0.48	1.48	1.62	1.88	-1.02	1.37	0.82
		NDBC-42036		NDBC-42039		All buoys		Satellite	
		ECMWF/ERA5	NCEP/NARR	ECMWF/ERA5	NCEP/NARR	ECMWF/ERA5	NCEP/NARR	ECMWF/ERA5	NCEP/NARR
U_{10}	**HH**	0.12	0.17	0.16	0.15	0.22	0.20	0.23	0.20
	NBIAS	0.05	0.12	0.04	0.07	-0.03	0.05	-0.03	0.02
Dir	**NRMSE**$_\theta$	3.91	1.75	4.45	2.41	5.52	3.94		
	NBIAS $_\theta$	3.14	0.82	3.93	1.92	2.08	0.77		

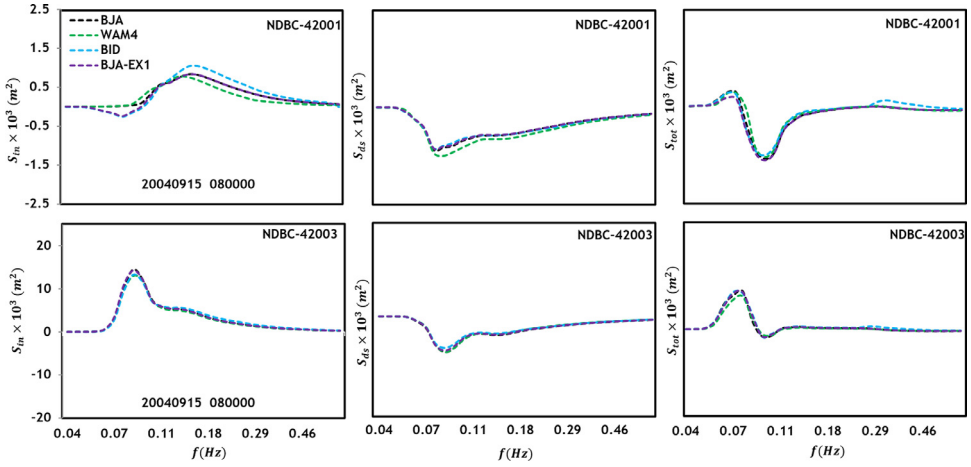

Figure 3 S_{in}, S_{ds} and S_{tot} values for the buoys 42001 and 42003 at 08:00 September 15th, 2004.

Table 3 Statistical parameters to evaluate H_s using ST3 at some buoy locations in the Gulf of Mexico and satellite data.

		NDBC-42001				NDBC-42003			
		BJA	WAM4	BID	BJA-EX1	BJA	WAM4	BID	BJA-EX1
H_s	HH	0.25	0.27	0.23	0.26	0.12	0.15	0.11	0.12
	NBIAS	-0.16	-0.18	-0.14	-0.18	-0.07	-0.11	-0.06	-0.07
		NDBC-42019				NDBC-42036			
		BJA	WAM4	BID	BJA-EX1	BJA	WAM4	BID	BJA-EX1
H_s	HH	0.33	0.33	0.36	0.35	0.13	0.15	0.13	0.13
	NBIAS	-0.17	-0.19	-0.19	-0.21	-0.09	-0.12	-0.08	-0.09
		All buoys				Satellite			
		BJA	WAM4	BID	BJA-EX1	BJA	WAM4	BID	BJA-EX1
H_s	HH	0.23	0.25	0.22	0.24	0.24	0.27	0.23	0.25
	NBIAS	-0.14	-0.17	-0.14	-0.16	-0.20	-0.26	-0.19	-0.21

Table 4 Statistical parameters to evaluate H_s using ST4 at some buoy locations in the Gulf of Mexico and satellite data.

		NDBC-42001						
		T405	T471	T471f	T471-EX1	T471-EX2	T471-EX3	T471-EX4
H_s	HH	0.30	0.15	0.18	0.15	0.14	0.13	0.12
	NBIAS	-0.24	-0.09	-0.12	-0.06	0.02	0.02	0.03
		NDBC-42003						
		T405	T471	T471f	T471-EX1	T471-EX2	T471-EX3	T471-EX4
H_s	HH	0.20	0.08	0.09	0.09	0.14	0.14	0.13
	NBIAS	-0.18	-0.03	-0.06	0.01	0.07	0.08	0.03
		NDBC-42036						
		T405	T471	T471f	T471-EX1	T471-EX2	T471-EX3	T471-EX4
H_s	HH	0.23	0.12	0.13	0.12	0.12	0.12	0.12
	NBIAS	-0.19	-0.05	-0.08	-0.02	0.03	0.04	0.05
		All buoys						
		T405	T471	T471f	T471-EX1	T471-EX2	T471-EX3	T471-EX4
H_s	HH	0.31	0.19	0.21	0.18	0.18	0.18	0.17
	NBIAS	-0.23	-0.10	-0.13	-0.07	-0.02	-0.01	-0.01
		Satellite						
		T405	T471	T471f	T471-EX1	T471-EX2	T471-EX3	T471-EX4
H_s	HH	0.31	0.20	0.22	0.19	0.19	0.20	0.19
	NBIAS	-0.34	-0.14	-0.18	-0.10	-0.05	-0.02	-0.03

When $f > f_p$, the wind and swell interaction was negligible at buoy 42001. The BID and BJA-EX1 formulations have different wave age tuning parameter z_α, which affects the spectrum for $f > f_p$; i.e. the S_{in} in the BID is higher than in the BJA-EX1. The dissipation term S_{ds} in BJA, BID and BJA-EX1 was similar for all frequencies. In contrast, the dissipation in WAM4 was greater across all frequencies which decreases S_{tot} and wave height. Comparison between simulation outputs and in situ data from NDBC- buoys and satellite data are shown in Table 3. The values of NBIAS indicate that all ST3 alternatives underestimated the wave height and period. Also, NBIAS values on the left side of hurricane is higher than values from the right side of the track. The HH values of the buoy data and the satellite data are also close to each other for all scenarios. The BID formulation had superior results to other ST3 alternatives.

4.3. Model assessment for ST4

From the variation of coefficients in ST4 variants, it can be inferred that the parameter β was the most important calibration parameter. Based on the NBIAS values (see Table 4), T405, T471 and T471 f underestimated H_s at almost all stations. Therefore, by increasing β, the amount of input energy can be increased, which led to increase in the wave height. A Newton—Raphson method was used to find the best β value to minimize the mean HH at all buoys and satellite data for wave height. The optimum value for β was estimated as 1.78 in T471-EX4, which also led to improved NBIAS values. The HH and NBIAS values at two buoys 42003 and 42036 for T471-EX1 and T471-EX4 showed that an increase in the β value from 1.55 to 1.78 led to increase in HH, which is unfavorable. Note that for buoys on the right side of the hurricane, due to the absence of the wave decay mechanism like swell dissipation and opposing wind, increasing the β parameter results in fast grow rate for Hs. In contrast, the grow rate of Hs by increasing β is relatively slow for buoys on the left side of the hurricane path such as 42002 and 42019. In Figure 4, the wave heights from model were compared with observations from 6 buoys during September 12 to 17, 2004.

The wave periods (Tm_{02}) at times of hurricane peak in all buoys were very close to NDBC data, while there are some differences in other times. Also, for the wave direction, whenever the angle between the wind and the waves reduced, the discrepancy between model and the measurements also reduced.

The T405 formulation significantly underestimated the wave height throughout the domain. Buoy 42003 was close to the hurricane center and located on the right side of the hurricane track; hence it experienced wave height as high as 11.04 m at 01:00 on September 15th. The ST4 alternatives, i.e. T471-EX4, T471-EX1, T471, T471 and T405 simulated H_s as 11.43, 10.92, 10.64, 10.25 and 9.04 m, respectively. The wind input term (S_{in}), dissipation term (S_{ds}) and the total source term (S_{tot}) at 09:00 on September 15, the time period when hurricane eye was close to buoys 42001 and 42003, are shown in Figure 5. Note that for T471, which differs from T471f only in β values, S_{in} values were

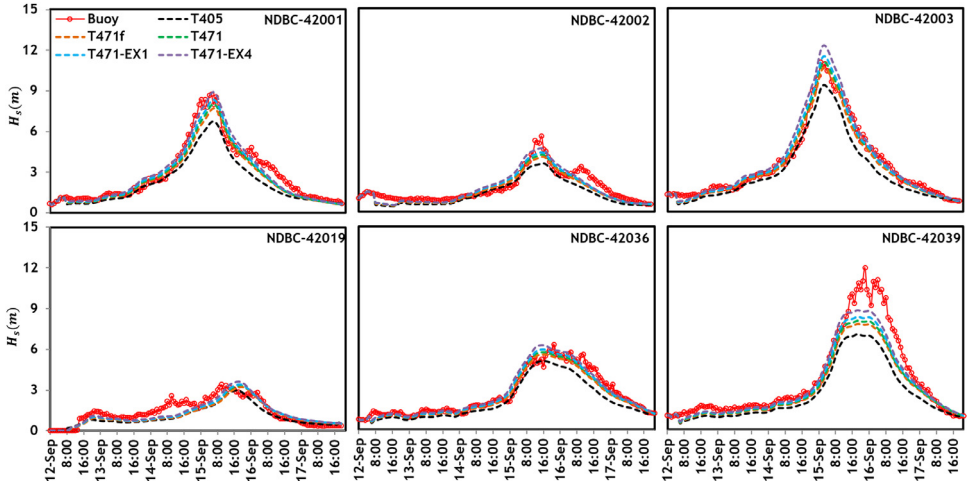

Figure 4 Comparisons of different tests in ST4 for calculating H_s at buoys in the Gulf of Mexico during Hurricane Ivan.

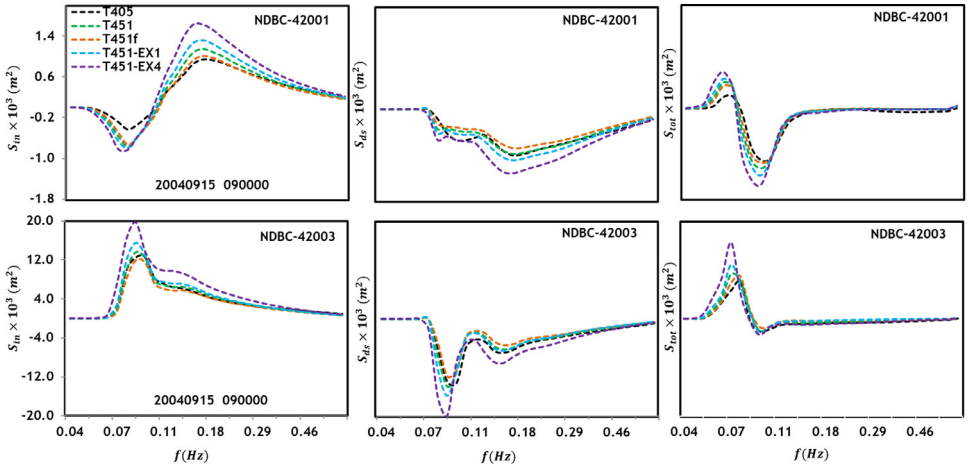

Figure 5 S_{in}, S_{ds} and S_{tot} values for the buoys 42001 and 42003 at 09:00 on September 15th, 2004.

greater at buoys 42001 and 42003. At the same time, the S_{ds} values were also higher in T471 than in T471f because both input and dissipation terms were defined as a function of the wave action spectrum $N(K, t)$. Finally, the values of S_{tot} were slightly higher in T471 than in T471f. This same was true for T471-EX1 and T471-EX4. The β values in T405, T471f and T471 were 1.55, 1.43 and 1.33, respectively. The S_{in} values are expected to be larger in T405 than in T471f and T471 (see Figure 5).

In contrast, as shown in Figure 4, the Hs was higher in all buoys when T471 test was employed. As shown in Figure 5, the values of S_{tot} in T471f and T471 are larger than those in T405 while opposite was true for S_{ds}. The added negative values of S_{ds} in T405 relative to T471 and T471f would ultimately reduce the S_{tot} value relative to T471 and T471f. Therefore, the necessary condition for increasing Hs is an increase in S_{in}, but this condition is not sufficient. Under certain environmental conditions and considering the coefficients that have been used in the model, stronger dissipation effects might be forced in the model, which would result in lower Hs. Since buoy 42003 was located on the right of the hurricane track with relatively larger wind speed, the S_{in} values are higher in 42003 than that in 42001. The same was true for S_{ds} and S_{tot} values at these two buoys. Note that the S_{in} was negative at 42001 at low frequencies (less than ~0.1 Hz) and the peak value of S_{in} occurred at 0.15 Hz. In contrast, the S_{in} values at buoy 42003 were always positive and the peak value of S_{in} was at low frequencies close to the peak frequency. The main reason for this difference was the presence of young swells at buoy 42001. The negative values of the swell dissipation term, S_{out} reduce the S_{in} in presence of swells throughout the spectrum. Therefore, if $S_{out} = 0$, the effects of the swell waves are ignored, and in this case, S_{in} value in buoy 42001 would have a positive value at all frequencies.

Based on NBIAS values presented in Table 4, the ST4 model with all selected configurations underestimated wave height at almost all stations. Comparing T451f and T405 indicated that β value is not the only important tuning parameter because the β value is higher in T405 than T451f, but underestimation was more evident in T405 than in T471f at all buoy locations. In other tests, increase in β value would make up for the wave height underestimation. The HH values at two buoys 42003 and 42036 for T471 and T471-EX3 show that an increase in the β value from 1.55 to 1.82 led to an increase in HH, which is unfavorable. Note that for

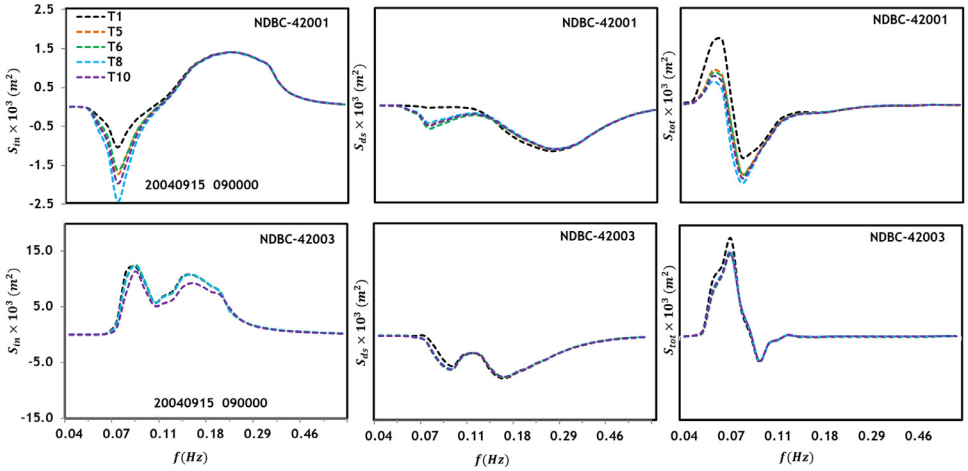

Figure 6 S_{in}, S_{ds} and S_{tot} value in the buoys 42001 and 42003 during 09:00 on September 15, 2004.

buoys on the right of the hurricane track, there is no efficient wave energy dissipation mechanism like swell dissipation. Therefore, increasing β cannot be done without a limit.

The NBIAS values in all tests were negative for T_{m02}, which indicated that the model underestimated wave period in all tests of ST4. Increasing the β parameter improved the HH for the peak period. In all T471 variants, HH values were larger for buoys located on the left side than the right side of hurricane track. The statistics were also almost similar for $NRMSE_\theta$. Therefore, based on statistical parameters for 6 buoys and satellite data, TEST451-EX4 is the most successful configuration for simulating wave height, peak period and wave direction in the Gulf of Mexico.

4.4. Model assessment for ST6

As mentioned in section 3.5, twelve scenarios were considered for ST6 package in which a_0 in Eq. (15) (the effect of opposing wind) and b_1 in Eq. (17) (the effects of wave dissipation due to the presence of swells) were changed. Increasing the coefficients a_0 and b_1 resulted in decreasing wave height simulated by the model. The two-dimensional Newton-Raphson method was used to find the optimum values for a_0 and b_1 that would minimize the mean HH at all buoys and satellite data for wave height. The best values for a_0 and b_1 were estimated in T12 as 0.11 and 0.0038, respectively.

The S_{in}, S_{ds} and S_{tot} values at buoys 42001 and 42003 at 09:00 on 15 September are presented in Figure 6. Increasing b_1 in T5 and T6 from 0.0032 to 0.0041 increased S_{in} at $f_p = 0.07$ Hz in buoy 42001 by 15%; while it decreased S_{ds} and S_{tot} by 35% and 19%, respectively. At buoy 42003, the increase in S_{in} was 6% at the peak frequency while decrease in $S_{ds}$and S_{tot} were 18% and 4%, respectively. It indicates that changing b_1 was more effective at buoy 42001. Negative values of S_{in} for low frequencies at buoy 42001 were highly sensitive to a_0 values such that increasing $a_0$would decrease S_{in} values. In contrast, it has negligible effects on S_{in} at high frequencies. Reducing a_0 values increased S_{tot}, especially close to the peak frequency. Changing the a_0 value has almost no effect on S_{in}, S_{ds} and S_{tot} at buoy 42003. The S_{in} values at this buoy were all positive due to a relatively small angle between mean wind and wave directions.

Comparing T5 and T8 shows that increasing a_0 from 0.09 to 0.14 increases S_{in} and S_{tot} at buoy 42001 by 44% and 180%, respectively and decreases S_{ds} by 7%. It can be concluded that the opposing wind and the presence of swells would effectively decrease H_s only at the buoys located on the left side of the hurricane track (e.g. buoy 42001).

The time series of wave height, wave period and wave direction showed that there is a fairly good agreement between the model and in situ observations (see Figure 7). The ST6 packages were relatively less accurate for buoys 42019, 42020 and 42039; most likely due to shallow water processes. At all buoys, the overestimation was observed when $H_s > 3$ m, while the model underestimated the wave height during fair weather condition.

The NBIAS values were relatively smaller in all tests for buoys at the left side of the hurricane track. The buoys 42002 and 42019 were located beyond the radius of the hurricane effect (R_{he}), and NBIAS were negative. The HH values are much lower for the buoys on the right side of the hurricane track than the corresponding values for the left-side buoys. For the right-side buoys, changing the a_0 value has negligible effects on the results because of small angle between wind and wave. In contrast, for buoys on the left of the hurricane track, the results highly depended on a_0 value. The T12 configuration has the best statistics in terms of reproducing wave height during study period against buoys and satellite data. Change in a_0 and b_1 coefficients had negligible effects on the wave direction and period of the wave.

The statistical parameters $NBIAS_\theta$ and $NRMSE_\theta$ presented in Table 5 show that error in buoys 42001 and 42003 are larger than those in other buoys. The wave direction in the buoys on the right side of the Hurricane Ivan (buoys 42003 and 42036) varies between 50 and 250°, while for the buoys on the left side of the track (42001, 42002 and 42019), the range is limited to ~70°. The wave period was suddenly increased on September 13 at buoys on the right side of the hurricane such as 42001, due to emergence of young swells from the previous location of the hurricane. As hurricane moved toward north of the Gulf of Mexico, the swells also

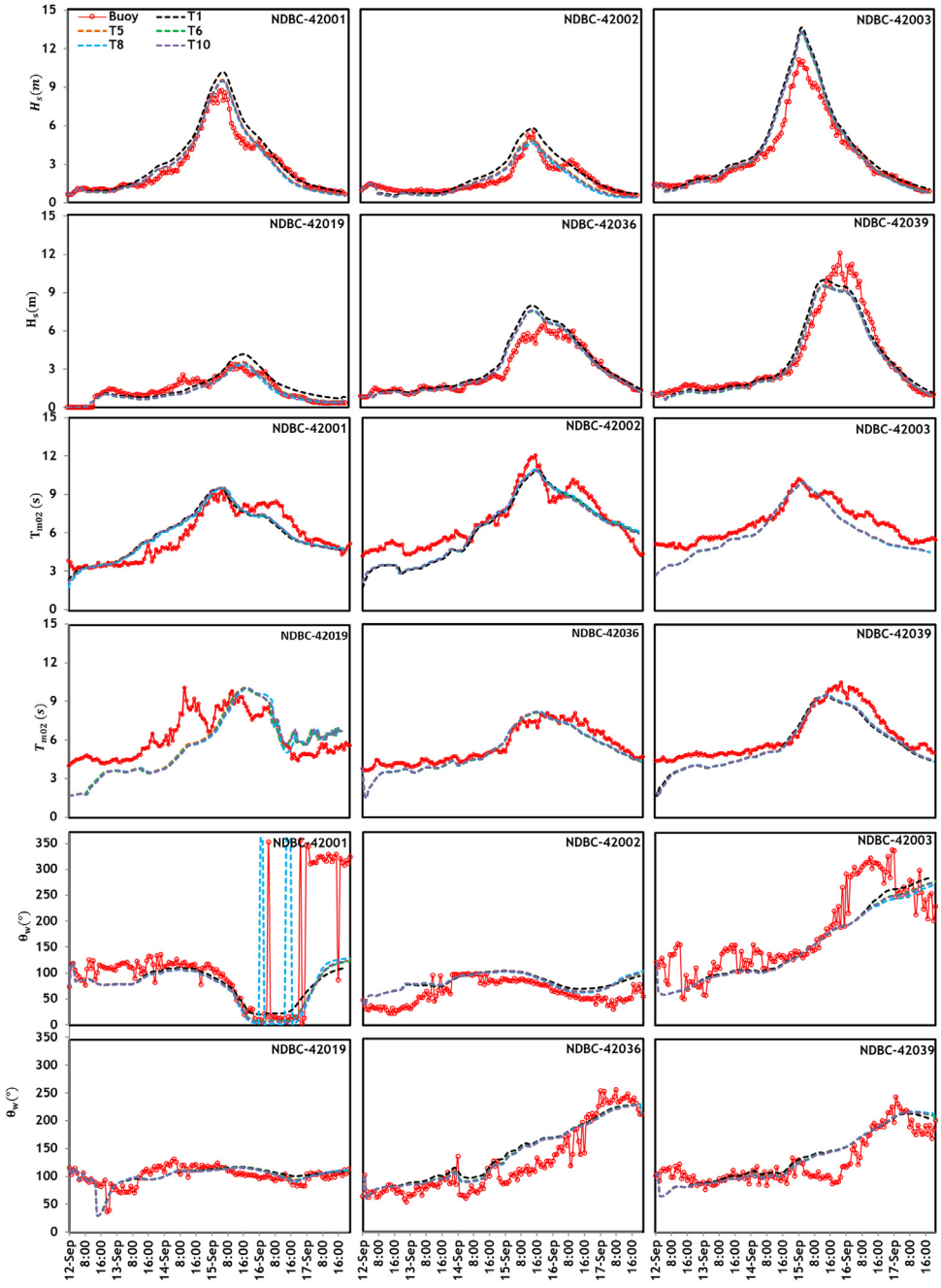

Figure 7 Comparisons between different tests in ST6 for calculating H_s, T_p and θ_w at buoys in the Gulf of Mexico during Hurricane Ivan.

propagated, and the same trend in wave period was also observed at other buoys such as 42019.

4.5. Comparison of source packages in WW3

The best configuration for each source package; i.e. BID, T471-EX4 and T12 as well as BJA, T471 and T6 as default configurations of ST3, ST4 and ST6 source packages were compared in terms of bulk wave parameters at buoys and satellite data locations using the Taylor diagram (see Figure 8). The Taylor diagram (Taylor, 2001) effectively summarizes statistical indices of correlation coefficient (CC), RMSE, Standard Deviation (SD). Each configuration is presented by a unique symbol on each diagram corresponding to different NDBC buoys. For buoys on the left of the hurricane track (42001, 42002 and 42019), the lowest CC corresponds to BJA (0.77) and the highest CC (0.94) corresponds to T471-EX4 and T12. Also BJA has the largest RMSE (1.10 m) while T471-EX4 showed the lowest RMSE (0.61 m). For buoys on the right of the hurricane track (42003, 42036 and 42039), the lowest CC corresponds to BJA (0.90) while T12 and T471-EX4 had the highest CCs (0.96 and 0.95). Also, BJA had the largest RMSE (1.11 m) while T471-EX4 showed the lowest RMSE (0.83 m). Therefore, T471-EX4 outperformed other configurations at buoys on the left of the hurricane while T12 had the best performance at other buoys.

Table 5 Statistical parameters for bulk wave parameters using different ST6 alternatives.

		NDBC-42001											
		T1	T2	T3	T4	T5	T6	T7	T8	T9	T10	T11	T12
	HH	0.21	0.17	0.17	0.2	0.16	0.15	0.19	0.15	0.16	0.16	0.15	0.15
H_s	NBIAS	0.17	0.09	0.08	0.13	0.06	0.04	0.09	0.03	0.04	0.05	0.03	0.04
	HH	0.13	0.13	0.13	0.13	0.13	0.13	0.12	0.13	0.12	0.13	0.13	0.13
T_{m02}	NBIAS	0.01	0.01	0.01	0.01	0.01	0.01	0.01	0.01	0.01	0.01	0.01	0.01
	NRMSE $_\theta$	9.76	9.93	9	9.57	9.2	9.05	9.52	10.15	9.68	9.64	9.69	9.62
θ_w	**NBIAS** $_\theta$	2.13	1.49	1.88	1.76	2.33	1.99	1.65	1.9	1.68	1.73	1.63	1.7
		NDBC-42002											
		T1	T2	T3	T4	T5	T6	T7	T8	T9	T10	T11	T12
	HH	0.29	0.26	0.22	0.25	0.23	0.23	0.25	0.25	0.28	0.23	0.24	0.22
H_s	NBIAS	0.18	0.07	0.04	0.07	-0.03	-0.06	-0.02	-0.1	-0.05	-0.05	-0.07	-0.06
	HH	0.15	0.16	0.16	0.16	0.15	0.15	0.16	0.15	0.16	0.16	0.16	0.16
T_{m02}	NBIAS	-0.09	-0.08	-0.09	-0.09	-0.09	-0.09	-0.09	-0.09	-0.09	-0.08	-0.08	-0.07
	NRMSE $_\theta$	3.8	3.82	3.67	3.76	3.74	3.68	3.75	3.86	3.78	3.77	3.78	3.77
θ_w	**NBIAS** $_\theta$	3.02	2.98	2.98	2.99	3.04	2.99	2.98	3.01	2.93	2.99	2.98	2.99
		NDBC-42003											
		T1	T2	T3	T4	T5	T6	T7	T8	T9	T10	T11	T12
	HH	0.22	0.19	0.18	0.22	0.19	0.19	0.22	0.19	0.16	0.19	0.19	0.18
H_s	NBIAS	0.18	0.13	0.11	0.17	0.12	0.11	0.17	0.12	0.12	0.12	0.11	0.11
	HH	0.16	0.16	0.15	0.15	0.16	0.16	0.16	0.16	0.16	0.16	0.16	0.16
T_{m02}	NBIAS	-0.13	-0.12	-0.12	-0.12	-0.13	-0.13	-0.13	-0.13	-0.12	-0.12	-0.12	-0.11
	NRMSE $_\theta$	6.94	7.17	7.04	7.06	6.89	7.01	7.11	7.03	7.18	7.09	7.13	7.1
θ_w	**NBIAS** $_\theta$	-3.61	-4.1	-3.62	-3.84	-3.32	-3.55	-3.91	-3.87	-3.91	-3.91	-3.99	-3.93
		NDBC-42019											
		T1	T2	T3	T4	T5	T6	T7	T8	T9	T10	T11	T12
	HH	0.29	0.27	0.27	0.25	0.25	0.26	0.24	0.27	0.35	0.25	0.26	0.25
H_s	NBIAS	0.09	-0.02	-0.05	-0.03	-0.12	-0.14	-0.11	-0.18	-0.16	-0.14	-0.12	-0.14
	HH	0.33	0.33	0.33	0.33	0.33	0.33	0.33	0.33	0.33	0.33	0.33	0.33
T_{m02}	NBIAS	-0.13	-0.13	-0.12	-0.12	-0.13	-0.13	-0.13	-0.13	-0.12	-0.13	-0.13	-0.12
	NRMSE $_\theta$	2.28	2.26	2.29	2.27	2.32	2.3	2.27	2.27	1.95	1.91	1.91	1.91
θ_w	**NBIAS** $_\theta$	0.01	-0.11	-0.04	-0.08	0.1	-0.02	-0.1	-0.05	0.01	0.09	0.08	0.09
		All buoys											
		T1	T2	T3	T4	T5	T6	T7	T8	T9	T10	T11	T12
	HH	0.24	0.21	0.21	0.22	0.2	0.2	0.22	0.21	0.22	0.2	0.2	0.19
H_s	NBIAS	0.13	0.05	0.03	0.08	0.01	-0.01	0.04	-0.02	-0.01	-0.01	-0.01	-0.01
	HH	0.17	0.17	0.17	0.17	0.17	0.17	0.17	0.17	0.17	0.17	0.17	0.17
T_{m02}	NBIAS	-0.09	-0.08	-0.08	-0.08	-0.09	-0.09	-0.09	-0.09	-0.08	-0.08	-0.08	-0.07
	NRMSE $_\theta$	5.24	5.26	5.06	5.17	5.15	5.08	5.16	5.32	5.15	5.13	5.14	5.12
θ_w	**NBIAS** $_\theta$	0.88	0.55	0.73	0.67	1.02	0.8	0.61	0.75	0.62	0.68	0.63	0.66
		Satellite											
		T1	T2	T3	T4	T5	T6	T7	T8	T9	T10	T11	T12
	HH	0.25	0.25	0.24	0.25	0.24	0.24	0.26	0.25	0.25	0.24	0.24	0.23
H_s	NBIAS	0.09	-0.03	0.01	0.05	-0.01	-0.03	0.03	-0.03	-0.07	-0.02	-0.03	-0.01

Taylor diagram for satellite data during this time period (Figure 8c) shows that T471-EX4 and T12 have the largest CC (0.97, 0.96) and the lowest RMSE (0.70, 0.56 m). The performance of all configurations were comparable for wave period (Figure 8d) but T471-EX4 was slightly more accurate than other configurations. In sum, T471-EX4 showed the best performance for simulating wave height under hurricane Ivan condition.

The distribution of mean NBIAS and HH values at all buoys for different wave height range and wave period are illus-

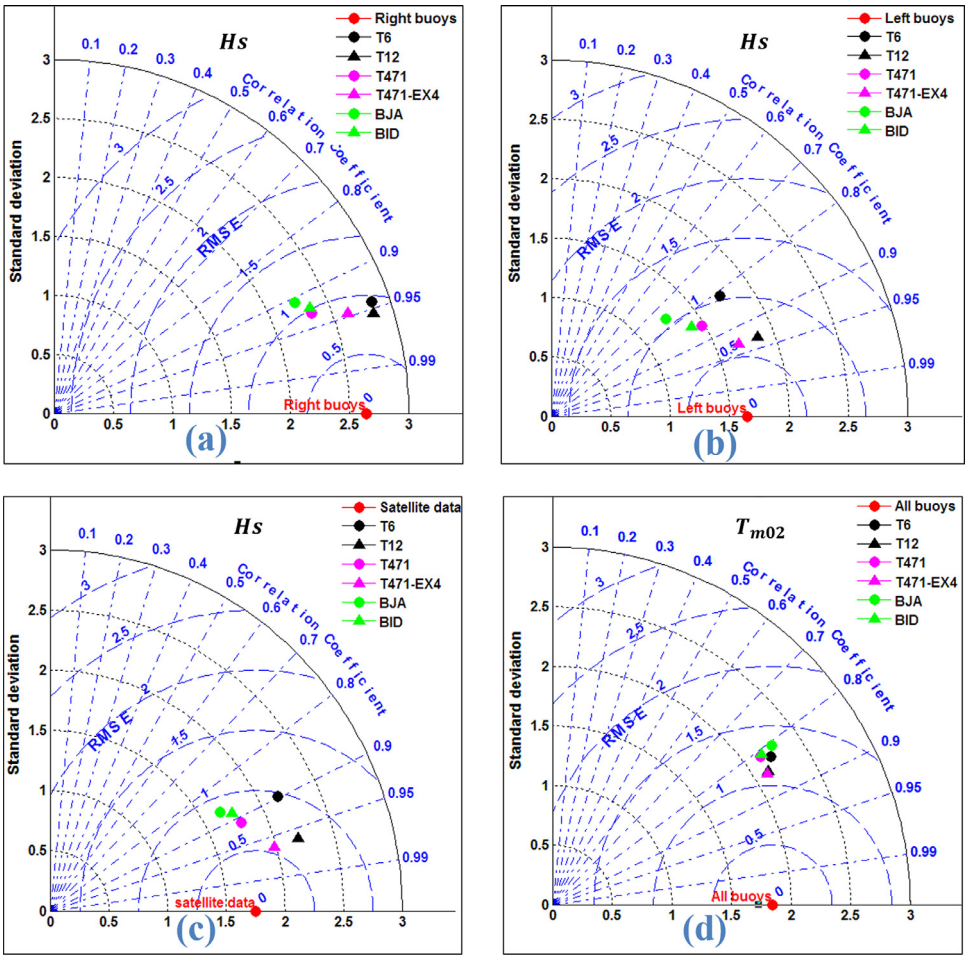

Figure 8 Taylor diagram for H_s at buoys on the right of hurricane track (a), from buoys on the left of hurricane track (b), from satellite data (c) and T_{02} at all buoys (d), in the Gulf of Mexico during Hurricane Ivan.

trated in Figure 9. When $H_s \leq 3$ m, which includes about 70% of the data during study period, the T471-Ex4 has the least underestimation of Hs. The T12 formulation overestimated the wave height when $H_s \geq 3$ m, while T471-Ex4 formulation underestimated the wave height in all ranges. HH values show that when $H_s < 6$ m, T471-EX4 was the best configuration while T12 outperformed other configurations when $H_s > 6$ m.

The model was more successful in reproducing wave period for long waves than for short waves. When $T_{m02} < 2.5s$, T471-EX4 was more successful while for $T_{m02} \geq 2.5s$, the T12 option was the best. Therefore, to simulate wave height and wave period under hurricane conditions and at particular points located within the radius of the hurricane effect (R_{he}), T12 is recommended. For fair weather conditions and also for the area beyond R_{he} during hurricane conditions, the T471-Ex4 is more appropriate.

5. Discussion

5.1. Effect of following and opposing wind fields during a hurricane passage

Wind and wave directions are almost aligned in the right front quarter of an advancing hurricane; while they are in reverse alignment on the left side of the track. The difference between the wind and wave directions can be evaluated using the relation proposed by Donelan et al. (1997) and Holthuijsen et al. (2012) where $\Delta\theta_{uw} = \min(|\theta_u - \theta_{wp}|360^\circ - |\theta_u - \theta_{wp}|)$. Using this definition, there is wind sea (hereafter WS) or following swell (hereafter FS) when $\theta_{uw} \leq 45^\circ$, cross swell (hereafter CS) when $45^\circ < \Delta\theta uw < 135^\circ$ and opposing swell (hereafter OS) when $\theta_{uw} \geq 135^\circ$. Liu et al (2017) divided CS into two parts: with $\Delta\theta_{uw} \in [45^\circ, 90^\circ]$ (hereafter CSP), and with $\Delta\theta_{uw} \in [90^\circ, 135^\circ]$ (hereafter CSN).

In Figure 10, rotating wind velocity vectors around the hurricane eye at 09:00 on September 15 is shown when hurricane path was directed to 325°N. The highest wind speeds occurred in the NE quadrant where the most extreme waves were generated. A blue symbol shows the eye of hurricane at this time, and the red symbol shows location of eye at earlier hours. Blue curved lines indicate locally generated wind seas at current time and red curved lines indicate young swells generated a few hours earlier from southeast, from the previous of the hurricane. FS occurs where red and blue lines have the same direction of propagation (NE of eye), CS occurs where red and blue lines are perpendicular to each other (NW and SE of eye) and OS occurs where red and blue lines are in opposite direction (S of eye). At this

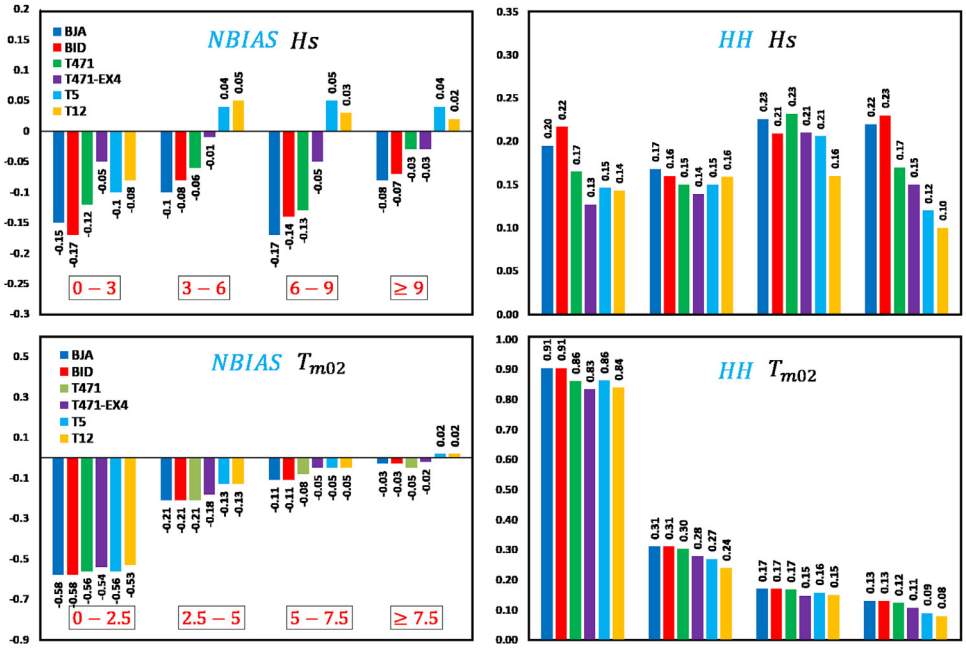

Figure 9 The column chart of the NBIAS and HH values for comparing H_s and T_{02} in tests BJA, BID, T471, T471-EX4, T5 and T12.

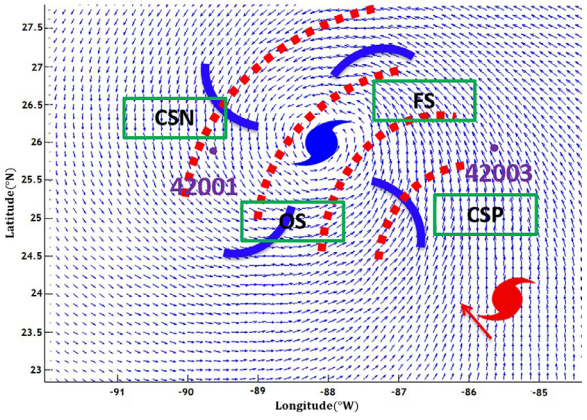

Figure 10 Wind/wave characteristics of Hurricane Ivan at 09:00 UTC on September 15 in the Gulf of Mexico. Blue arrows show wind vector, A blue symbol and red symbol indicate the location of an eye of the hurricane at this time and earlier hours. Blue curved lines and red curved lines indicate wind sea and young swells. Purple circles are the locations of buoys 42001 and 42003.

time, buoy 42003 experienced FS and buoy 42001 experienced CF cases.

Figure 11 compares the time series of direction of wind and wave from 6 buoys while hurricane Ivan was active in the Gulf of Mexico. For the left side buoys, the direction of wind and wave are close together until a certain time. When the hurricane would pass by the buoy locations, the difference in direction of wind and wave would increase and the buoys located on left side of hurricane experienced CS and OS cases. In contrast, for the right side buoys, the directions of wind and wave were almost the same, and most often, these buoys experienced FS and CS case.

5.2. Wave attenuation d as a function of wind and wave directions

It is clear from Eq. (13) and Eq. (15) that the wave growth depends on the wave age and the difference between the wind and wave angles, such that W is equal to the sum of the following wind effects W_1 and the opposing wind effects W_2. Donelan (1999) investigated the wave growth in laboratory conditions and proposed the following equation for calculating the wave growth:

$$\gamma(f) = s\left(U_{\lambda/2}/C(f) - 1\right)\left|U_{\lambda/2}/C(f) - 1\right| \tag{22}$$

$$s = \begin{cases} 0.28 \ for \ U_{\lambda/2}/C(f) \geq 1 \\ 0.11 \ for \ U_{\lambda/2}/C(f) < 1 \end{cases} \tag{23}$$

where $U_{\lambda/2}$ is the wind speed at the height of one-half of the wavelength λ, C is the phase speed, s is the so-called sheltering coefficient. For $U_{(\lambda/2)}/C(f) < 1$, the sheltering coefficient was estimated for swells travelling exactly under opposing winds i.e., *OS* and no information for *CS* case was presented. Note that s values in Eq. (23) implies that the rate of wave growth is $\frac{0.28}{0.11} \approx 2.5$ times as high as the wave attenuation. Donelan et al. (2012) proposed another set of sheltering coefficients for γ using University of Miami Wave Model that considered the angle between wind and wave direction.

$$\gamma(f) = s\left(U_{\lambda/2}/C(f)\cos(\Delta\theta_{uw}) - 1\right)\left|U_{\lambda/2}/C(f)\cos(\Delta\theta_{uw}) - 1\right| \tag{24}$$

$$s = \begin{cases} 0.11 \ for \ U_{\lambda/2}/C(f)\cos(\Delta\theta_{uw}) \geq 1 \\ 0.01 \ for \ 0 \leq U_{\lambda/2}/C(f)\cos(\Delta\theta_{uw}) \leq 1 \\ 0.10 \ for \ U_{\lambda/2}/C(f)\cos(\Delta\theta_{uw}) \leq 0 \end{cases} \tag{25}$$

Hence, the attenuation rate of CSN and OS (when $U_{\lambda/2}/C(f)\cos(\Delta\theta_{uw}) \leq 0$) and CSP when

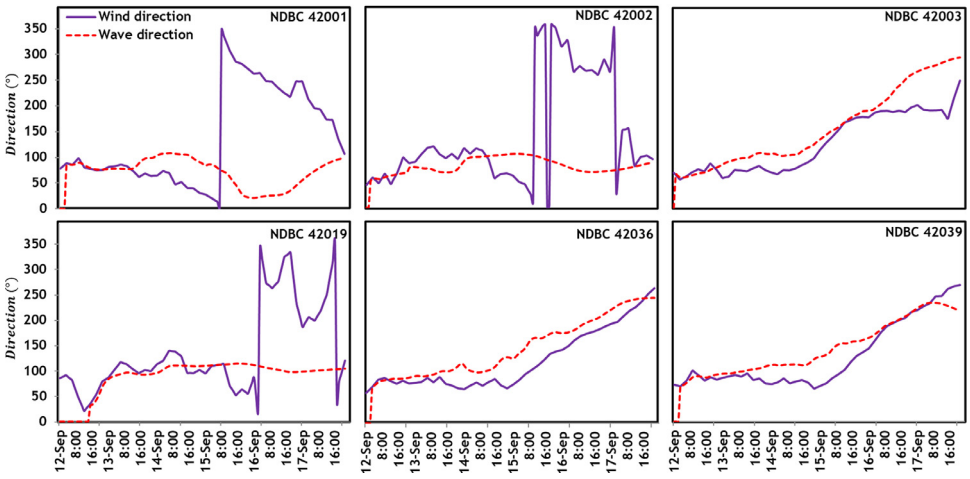

Figure 11 Comparison of wind and wave direction time series at buoys in the Gulf of Mexico during Hurricane Ivan.

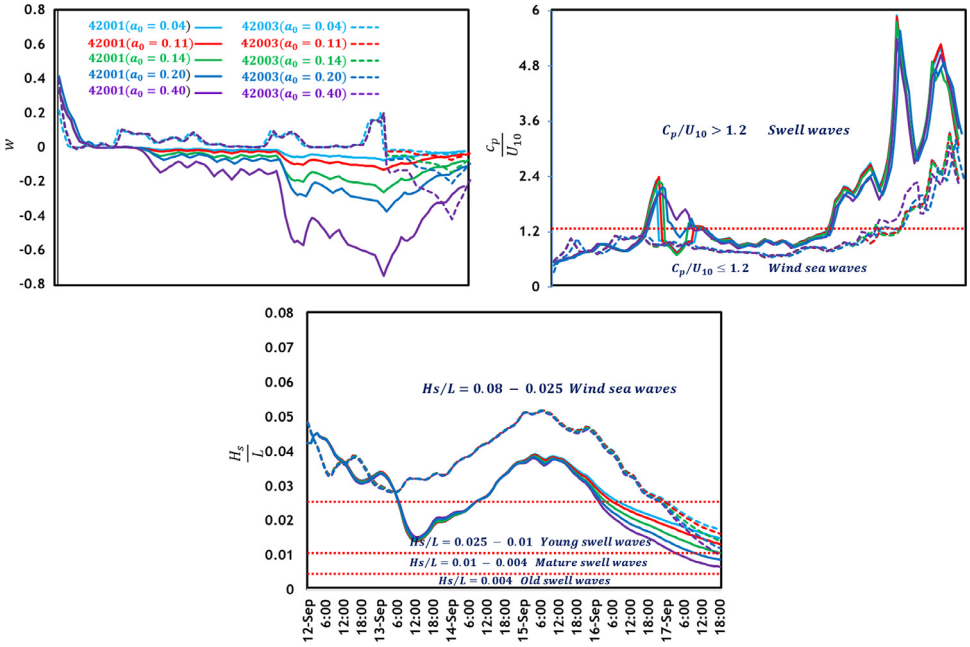

Figure 12 Effect of a_0 value on wave steepness, wave age and W at buoys 42001 and 42003.

$(0 \le U_{\lambda/2}/C(f)\cos(\Delta\theta_{uw}) \le 1)$ are $0.91(0.10/0.11 \approx 0.91)$ and $0.01/0.11 \approx 0.09$ of the growth rate of *OS* (when $U_{\lambda/2}/C(f)\cos(\Delta\theta_{uw}) \le 0$). Such variation should be included in the a_0 value in the model.

In contrast, a fixed value is suggested for a_0 in ST6 formulation. To address this problem, five values of 0.04, 0.11, 0.14, 0.20 and 0.4 were tested for a_0 in combination with constant value of $b_1 = 0.0038$. In Figure 12, the values of W, the wave steepness H_s/L and wave age C_p/U_{10} for buoys 42003 and 42001, corresponding to different a_0 values, are presented while the Hurricane Ivan traversed through the Gulf of Mexico. At buoy 42001, W was positive in the first part of the diagram; i.e. energy was transferred from the wind to the wave. As the hurricane approached and passed close to the buoy at 09:00 UTC September 15, the W value became negative for all a_0 values, indicating dissipated wave growth and energy transfer from the wave to the wind. At buoy 42003, when the storm passed close to the buoy, $\cos(\Delta\theta_{uw})$ was a positive value and W was significantly increased as a result of increasing the ratio of wind speed to the wave speed, and decreasing the angle between wind and wave. The dimensionless parameters of wave steepness H_s/L, and wave age C_p/U_{10} are used to determine the nature of the sea state. Thomson et al. (2013) divided the ocean waves into four modes according to the wave steepness as $H_s/L = 0.080 - 0.025$ for the wave sea, $H_s/L = 0.025 - 0.01$ for young swell waves, $H_s/L = 0.01 - 0.004$ for mature swell waves, and $H_s/L = 0.004$ for old swell waves. The wave age can also be employed to define the sea condition when $C_p/U_{10} \le 1.2$, and swells when $C_p/U_{10} > 1.2$ (Alves et al., 2003; Pierson and Moskowitz, 1964) . Hence, waves at buoy 42001 were generally considered older than the waves at buoy 42003, and the wave steepness was relatively lower. Also, about 85% of the waves at buoy 42003 were wind sea and the remaining 15% were combined sea and swells occurred on September 17. In contrast, 48% of the waves at

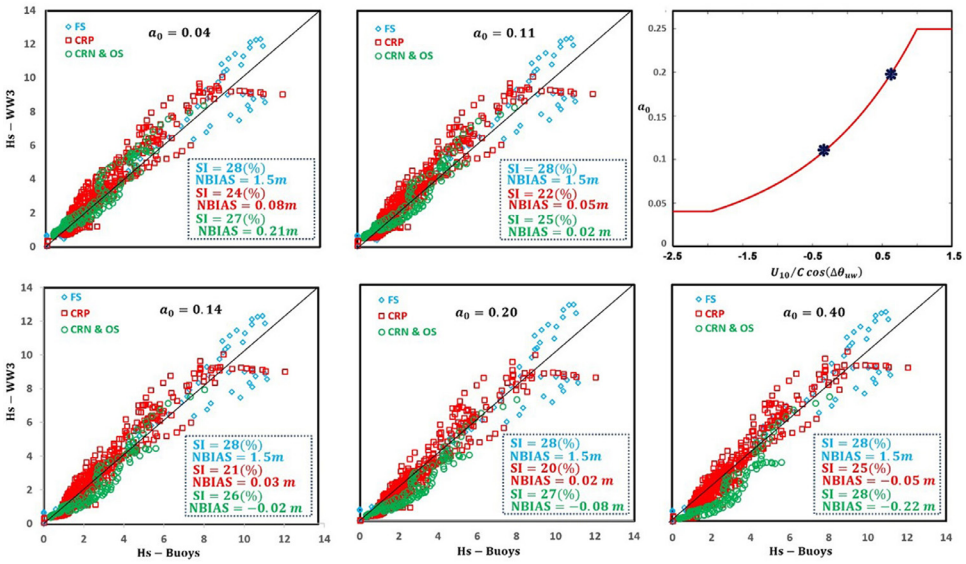

Figure 13 Scatter plot of model H_s during Hurricane Ivan in FS, CS, and OS cases against observations.

Table 6 Statistical parameters to compare H_s in T12 and a new model $ST6^m$ at buoys locations in the Gulf of Mexico and satellite data.

	NDBC-42001		NDBC-42002		NDBC-42003		NDBC-42019	
	ST6	^{m}ST6	ST6	^{m}ST6	ST6	ST6	ST6	^{m}ST6
HH	0.17	0.18	0.20	0.19	0.16	0.16	0.23	0.22
NBIAS	0.05	0.06	-0.02	-0.01	0.10	0.10	-0.10	-0.09
	NDBC-42036		NDBC-42039		All Buoys		Satellite	
	ST6	^{m}ST6	ST6	^{m}ST6	ST6	ST6	ST6	^{m}ST6
HH	0.18	0.18	0.15	0.14	0.19	0.18	0.23	0.22
NBIAS	0.10	0.10	-0.04	-0.03	0.02	0.01	0.02	0.01

locations in the Gulf of Mexico and satellite data.

buoy 42001 were a combination of swell and wind sea. It is noted that when the Hurricane Ivan was close to the buoys, due to rapid increase of wind speed relative to the wave phase speed, the wind sea dominated the sea state. At both buoy locations changes were fairly similar until 04:00 on September 13; however, at buoy 42001, the wave age was suddenly increased due to presence of young swells and the wave steepness reached a value less than 0.025 thereafter. At buoy 42003, the increase in wave age was low, and the presence of young swells was not noticeable in the wave steepness.

Appearance of more young swell at buoy 42001 than buoy 42003 can be justified as follows: the young swell was produced under the influence of the Hurricane Ivan even before it reached the buoys. Considering the angle of hurricane track (325°) and the high wave phase speed compared to the hurricane translation velocity (∼10 vs. ∼4 m/s), these waves would reach buoys 42001 and 42003 much earlier than arrival of hurricane eye. The larger distance of buoy 42001 relative to buoy 42003 from the track of Hurricane Ivan center results in lower steepness of propagated waves at buoy 42001; hence, it experienced young swell from 10:00 September 13 to 10:00 September 14. The same occurred for buoys 42002 and 42019 during later hours. The change in the coefficient a_0 did not affect the wave steepness and wave age; while increasing a_0 would decrease the wave steepness and wave age at buoy 42001.

5.3. Numerical experiments to assess model performance with variable a_0

As mentioned in section 5.2, a constant value is used for a_0 in WW3. During the passage of Hurricane Ivan, all buoys in the Gulf of Mexico experienced the FS, CSP, CSN, or OS cases at different time periods. On the other hand, different a_0 values were used in different experimental setups presented in Table 1. Therefore, to select the best value for a_0 for all different cases, hourly model results at buoy locations during study period were classified as FS, CSP, CSN, or OS cases. It can be showed that ∼19% of the waves were FS case, ∼66% were CSP case and 15% were CSN case. The scatter plot of model results using T12 formulation at all NDBC buoys are presented in Figure 13 for different a_0 values. The SI and NBIAS indices indicate that changing the parameter a_0 has no effect on the wave height in the FS case. The best statistics for CSP occurred when $a_0 = 0.2$ ($SI = 20\%$

and NBIAS = 0.02) whereas for CSN or OS case in which $a_0 = 0.11$ ($SI = 25\%$ and NBIAS = 0.02 m) was the optimum value. It implies that by increasing the angle between the wave and wind, it is necessary to use a smaller value for a_0. By drawing the best fit-line from three values of $a_0 = 0.11$, 0.20 and asymptotic value of 0.25 according to Figure 13, a general exponential relationship can be deduced as $a_0 = \max\{0.04,\ 0.134 \exp[0.62 \times \min(1, \frac{U_{10}}{C} \cos(\Delta\theta_{uw}))]\}$.

Implementing the proposed equation for a_0 in the source of the WW3 led to a new source term package $ST6^m$. A comparison between the NBIAS and HH results of the wave height for $ST6^m$ and T12 are shown in the Table 6. For the buoys located on left side of the hurricane path that experienced CS and OS cases, wave height values were increased because the $ST6^m$ uses a lower value of a_0. In contrast, almost no change was seen at buoys on the right of the hurricane track. Overall, use of a more suitable value for a_0 in the $ST6^m$ configuration improved the model performance. The statistical indices both for NDBC buoys and satellite data show superior performance of $ST6^m$ than ST6-T12 for wave height. More improvement in results are expected for slow moving hurricanes such as Hurricane Isaac (2012) than Hurricane Ivan (2004) because of longer CS and OS periods.

6. Conclusions

Turbulent sea state and other fluctuating physical conditions during the passage of a strong hurricane, such as rapid change in wind speed and direction, make hurricane modeling a challenging test for different source packages in WW3. In this study, NCEP/NARR wind data for hurricane Ivan were used after implementing a data assimilation. Several variants of ST3, ST4 and ST6 packages were employed to assess the model performance against in situ data from NDBC buoys as well as satellite data. The important findings of this research are summarized as follows:

- Comparing the wind data extracted from NCEP/NARR and ECMWF/ERA5 with NDBC buoys data and satellite data show that NCEP/NARR slightly overestimated the wind speed, while ECMWF/ERA5 underestimated it. Statistical indices showed slightly better performance of NCEP/NARR in the Gulf of Mexico.
- Among ST3 alternatives, the BID configuration had superior results due to inclusion of the swell parameter s_1. The HH and NBIAS values for simulating wave height using BID configuration were ~5% and ~4% smaller than corresponding values using default configuration of the model.
- In ST4 source package, the parameter β was the most important tuning parameter such that by increasing β, the amount of input energy would be increased, which led to increase in the wave height. In this research, A Newton—Raphson method was used to find the optimum value for β to minimize the mean HH. The outcome of this process was β=1.78 which led to T471-EX4 configuration. The HH value for simulating wave height using T471-EX4 configuration were ~5—10% smaller than corresponding values using default configuration of the model. The NBIAS becomes ~0 using T471-EX4.
- Increasing β increases all three terms S_{in}, S_{ds} and S_{tot} but the increase in S_{in} is more than other terms. For buoys on the right side of the hurricane, increasing the β parameter results in fast grow rate of wave height due to absence of the wave decay mechanism like swell dissipation and opposite wind. In contrast, the grow rate of wave height by increasing β would be slow for buoys on the left side of the hurricane.
- For the ST6 package, increasing the coefficients a_0 and b_1 decreases the wave height predicted by the model. Optimization showed that $a_0 = 0.11$ and $b_1 = 0.0038$ were optimal values for Hurricane Ivan (called T12). The NBIAS becomes ~0 for wave height and the HH value was improved by ~5% compared to default configuration of the model. The model overestimation was observed when $H_s > 3$ m while the model underestimated the wave height during fair weather condition.
- Change in a_0 and b_1 coefficients in ST6 and β in ST4 had negligible effects on the wave direction and wave period. Although there was a fair agreement between simulation results and observed data; however, the model was more successful in reproducing the wave period at times near hurricane peak.
- Comparison between the results of WW3 models and the measured data (NDBC buoys and satellite data) show that closer to hurricane eye, T12 was the most successful formulation. In fair weather condition and beyond R_{he} during hurricane condition, the T471-Ex4 is more appropriate
- Changing the parameter a_0 has no effect on the wave height in the FS case. The best value of a_0 for CSP case is 0.20 and for CSN or OS cases is 0.11; hence, by increasing the angle between the wave and wind, it is necessary to use a larger value for a_0. To address this point, a parametric formulation for a_0 was suggested which improved the model performance.

References

Allard, R., Rogers, E., Martin, P., Jensen, T., Chu, P., Campbell, T., Dykes, J., Smith, T., Choi, J., Gravois, U., 2014. The US Navy Coupled Ocean-Wave Prediction System. Oceanography 27 (3), 92—103. https://doi.org/10.5670/oceanog.2014.71

Alves, J.-H., Banner, M.L., Young, I., 2003. Revisiting the Pierson—Moskowitz Asymptotic Limits for Fully Developed Wind Waves. J. Phys. Oceanogr. 33 (7), 1301—1323. https://doi.org/10.1175/1520-0485(2003)033⟨1301:RTPALF⟩2.0.CO;2

Ardhuin, F., Chapron, B., Collard, F., 2009. Observation of swell dissipation across oceans. Geophys. Res. Lett. 36 (6), L06607. https://doi.org/10.1029/2008GL037030

Ardhuin, F., Jenkins, A., 2006. On the Interaction of Surface Waves and Upper Ocean Turbulence. J. Phys. Oceanogr. 36 (3), 551—557. https://doi.org/10.1175/JPO2862.1

Ardhuin, F., Rogers, E., Babanin, A.V., Filipot, J.-F., Magne, R., Roland, A., van der Westhuysen, A., Queffeulou, P., Lefevre, J.-M., Aouf, L., Collard, F., 2010. Semiempirical Dissipation Source Functions for Ocean Waves. Part I: Definition, Calibration, and Validation. J. Phys. Oceanogr. 40 (9), 1917—1941. https://doi.org/10.1175/2010JPO4324.1

Babanin, A., 2006. On a wave-induced turbulence and a wave-mixed upper ocean layer. Geophys. Res. Lett. (20). https://doi.org/10.1029/2006GL027308

Babanin, A., 2009. Breaking of ocean surface waves. Acta. Phys. Slovaca. 59 (4), 305—535. https://doi.org/10.2478/v10155-010-0097-5

Babanin, A., 2011. Breaking and Dissipation of Ocean Surface Waves. Cambridge University Press.

Babanin, A., Chalikov, D., 2012. Numerical investigation of turbulence generation in non-breaking potential waves. J. Geophys. Res. 117 (C11). https://doi.org/10.1029/2012JC007929

Babanin, A., Solov'yev, Y.P., 1987. Parameterization of the width of the angular distribution of wind wave energy at limited fetches. Izv. Atmos. Ocean. Physics. 23, 645–651.

Babanin, A., Tsagareli, K., Young, I., Walker, D., 2007. Implementation of New Experimental Input/Dissipation Terms for Modelling Spectral Evolution of Wind Waves.

Babanin, A., Tsagareli, K., Young, I., Walker, D., 2010. Numerical Investigation of Spectral Evolution of Wind Waves. Part II: Dissipation Term and Evolution Tests. J. Phys. Oceanogr. 40 (4), 667–683. https://doi.org/10.1175/2009JPO4370.1

Babanin, A., Westhuysen, A., 2008. Physics of "Saturation-Based" Dissipation Functions Proposed for Wave Forecast Models. J. Phys. Oceanogr. 38 (8), 1831–1841. https://doi.org/10.1175/2007JPO3874.1

Babanin, A., Young, I., 2005. Two-phase behaviour of the spectral dissipation of wind waves. Ocean Waves Measurement and Analysis, Madrid, Spain.

Belcher, S.E., Hunt, J.C.R., 1993. Turbulent shear flow over slowly moving waves. J. Fluid. Mech. 251, 109–148. https://doi.org/10.1017/S0022112093003350

Beyramzade, M., Siadatmousavi, S.M., 2019. Skill assessment of SWAN model in the red sea using different wind data. Reg. Stud. Mar. Sc. https://doi.org/10.1016/j.rsma.2019.100714

Bi, F., Song, J., Wu, K., Xu, Y., 2015. Evaluation of the simulation capability of the Wavewatch III model for Pacific Ocean wave. Acta. Oceanol. Sin. 34 (9), 43–57. https://doi.org/10.1007/s13131-015-0737-1

Bidlot, J., Janssen, P., Abdalla, S., Hersbach, H., 2007. A revised formulation of ocean wave dissipation and its model impact ECMWF. ECMWF Technical Memoranda.

Booij, N., Ris, R., Holthuijsen, L., 1999. A third-generation wave model for coastal regions, Part I, Model description and validation. J. Geophys. Res. 104 (C4), 7649–7656. https://doi.org/10.1029/98JC02622

Brenner, S., Gertman, I., Murashkovsky, A., 2007. Preoperational ocean forecasting in the southeastern Mediterranean Sea: Implementation and evaluation of the models and selection of the atmospheric forcing. J. Mar. Syst. 65 (1), 268–287. https://doi.org/10.1016/j.jmarsys.2005.11.018

Cavaleri, L., Sclavo, M., 2006. The calibration of wind and wave model data in the Mediterranean Sea. Coast. Eng. 53 (7), 613–627. https://doi.org/10.1016/j.coastaleng.2005.12.006

Chao, Y., Alves, J.-H., Tolman, H., 2005. An Operational System for Predicting Hurricane-Generated Wind Waves in the North Atlantic Ocean. Weather Forecast 20 (4), 652–671. https://doi.org/10.1175/WAF851.1

Cheng, Z., Mitsuyasu, H., 1992. Laboratory studies on the surface drift current induced by wind and swell. J. Fluid. Mech. 243, 247–259. https://doi.org/10.1017/S0022112092002714

Christakos, K., Björkqvist, J.-V., Tuomi, L., Furevik, B.R., Breivik, Ø., 2020. Modelling wave growth in narrow fetch geometries: The white-capping and wind input formulations. Ocean. Model. 157, 101730. https://doi.org/10.1016/j.ocemod.2020.101730

Donelan, A.M., Pierson, J.W., 1987. Radar Scattering and Equilibrium Ranges in Wind-Generated Waves With Application to Scatterometry. J. Geophys. Res. 92 (C5), 4971–5029. https://doi.org/10.1029/JC092iC05p04971

Donelan, M., Babanin, A., Young, I., Banner, M., 2006. Wave-Follower Field Measurements of the Wind-Input Spectral Function. Part II: Parameterization of the Wind Input. J. Phys. Oceanogr. 36 (8), 1672–1689. https://doi.org/10.1175/JPO2933.1

Donelan, M., Babanin, A., Young, I., Banner, M.L., McCormick, C., 2005. Wave-Follower Field Measurements of the Wind-Input Spectral Function. Part I: Measurements and Calibrations. J. Atmos. Oceanic. Tech. 22 (7), 799–813. https://doi.org/10.1175/JTECH1725.1

Donelan, M., Curcic, M., Chen, S., Magnusson, A., 2012. Modeling waves and wind stress. J. Geophys. Res. (C11). https://doi.org/10.1029/2011JC007787

Donelan, M., Drennan, W., Katsaros, K., 1997. The Air–Sea Momentum Flux in Conditions of Wind Sea and Swell. J. Phys. Oceanogr. 27 (10), 2087–2099. https://doi.org/10.1175/1520-0485(1997)027⟨2087:TASMFI⟩2.0.CO;2

Donelan, M.A., 1999. Wind-Induced Growth and Attenuation of Laboratory Waves. In: Sajjadi, S.G., Thomas, N.H., Hunt, J.C.R. (Eds.), Wind-over-Wave Couplings: Perspectives and Prospects. Clarendon, 183–194.

Donelan, M.A., Haus, B., Reul, N., Plant, W., Stiassnie, M., Graber, H., Brown, O., Saltzman, E., 2004. On the limiting aerodynamic roughness of the ocean in very strong winds. Geophys. Res. Lett. 31 (18). https://doi.org/10.1029/2004GL019460

Fan, Y., Ginis, I., Hara, T., Wright, C.W., Walsh, E.J., 2009. Numerical Simulations and Observations of Surface Wave Fields under an Extreme Tropical Cyclone. J. Phys. Oceanogr. 39 (9), 2097–2116. https://doi.org/10.1175/2009JPO4224.1

Hanna, S.R., Heinold, D.W., 1986. Simple Statistical Methods for Comparative Evaluation of Air Quality Models. In: De Wispelaere, C., Schiermeier, F.A., Gillani, N.V. (Eds.), Air Pollution Modeling and Its Application V. Springer US, Boston, MA, 441–452.

Hanson, J., Tracy, B., Tolman, H., Scott, R., 2009. Pacific Hindcast Performance of Three Numerical Wave Models. J. Atmos. Oceanic. Tech. 26 (8), 1614–1633. https://doi.org/10.1175/2009JTECHO650.1

Hasselmann, D., Bösenberg, J., 1991. Field measurements of wave-induced pressure over wind-sea and swell. J. Fluid. Mech. 230, 391–428. https://doi.org/10.1017/S0022112091000848

Hasselmann, K., Bauer, E., Janssen, P., Komen, G., Bertotti, L., Lionello, P., Guillaume, A., Cardone, V., Greenwood, J., Reistad, M., Zambresky, L., Ewing, J., 1988. The WAM model – a third generation ocean wave prediction model. J. Phys. Oceanogr. 18 (12), 1775–1810. https://doi.org/10.1175/1520-0485(1988)018⟨1775:TWMTGO⟩2.0.CO;2

Hasselmann, K., Lionello, P., Hasselmann, K., 1997. An optimal interpolation scheme for the assimilation of spectral wave data. J. Geophys. Res. 1021 (C7), 15823–15836. https://doi.org/10.1029/96JC03453

Holthuijsen, L., Powell, M., Pietrzak, J., 2012. Wind and waves in extreme hurricanes. J. Geophys. Res. 117 (C9), 9003. https://doi.org/10.1029/2012JC007983

Janssen, P., 1991. Quasilinear Theory of Wind-Wave Generation Applied to Wave Forecasting. J. Phys. Oceanogr. 21, 1631–1642. https://doi.org/10.1175/1520-0485(1991)021⟨1631:QLTOWW⟩2.0.CO;2

Janssen, P.A.E.M., 1982. Quasilinear approximation for the spectrum of wind-generated water waves. J. Fluid. Mech. 117, 493–506. https://doi.org/10.1017/S0022112082001736

Janssen, P.A.E.M., 2004. The Interaction of Ocean Waves and Wind, 1st edn. Cambridge University Press, Cambridge, UK.

Jiang, L., Zhang, Z., Qi, Y., 2010. Simulations of SWAN and WAVEWATCH III in northern south china sea. In: Proceedings of the International Offshore and Polar Engineering Conference. Beijing, China. International Society of Offshore and Polar Engineers.

Kalantzi, G., Gommenginger, C., Srokosz, M., 2009. Assessing the Performance of the Dissipation parameterizations in WAVEWATCH III Using Collocated Altimetry Data. J. Phys. Oceanogr. 39 (11), 2800–2819. https://doi.org/10.1175/2009JPO4182.1

Kazeminezhad, M.H., Siadatmousavi, S.M., 2017. Performance evaluation of WAVEWATCH III model in the Persian Gulf using different wind resources. Ocean. Dyn. 67 (7), 839—855. https://doi.org/10.1007/s10236-017-1063-2

Komen, G., Hasselmann, K., 1984. On the Existence of a Fully Developed Wind-Sea Spectrum. J. Phys. Oceanogr. 14, 1271—1285. https://doi.org/10.1175/1520-0485(1984)014⟨1271:OTEOAF⟩2.0.CO;2

Komen, G.J., Cavaleri, L., Donelan, M., Hasselmann, K., Hasselmann, S., Janssen, P.A.E.M., 1996. Dynamics and Modelling of Ocean Waves. Cambridge University Press.

Lakshmi H Kantha, C.A.C., 2000. Numerical models of oceans and oceanic processes. J. Fluid. Mech. 432, 442—442. https://doi.org/10.1017/S0022112001003822

Liu, Q., Babanin, A., Fan, Y., Zieger, S., Guan, C., Moon, I.-J., 2017. Numerical simulations of ocean surface waves under hurricane conditions: Assessment of existing model performance. Ocean. Model. 118, 73—93. https://doi.org/10.1016/j.ocemod.2017.08.005

Liu, Q., Rogers, W., Babanin, A., Young, I., Romero, L., Zieger, S., Qiao, F., Guan, C., 2018. Observation-based source terms in the third-generation wave model WAVEWATCH III: Updates and verification. J. Phys. Oceanogr. 49 (2), 489—517. https://doi.org/10.1175/JPO-D-18-0137.1

Mazaheri, S., Kamranzad, B., Hajivalie, F., 2013. Modification of 32 years ECMWF wind field using QuikSCAT data for wave hindcasting in Iranian Seas. J. Coast. Res. 65 (SP1), 344—349. https://doi.org/10.2112/SI65-059.1

Meissner, T., Smith, D., Fj, W., 2001. A 10-year intercomparison between collocated Special Sensor Microwave Imager oceanic surface wind speed retrievals and global analyses. J. Geophys. Res. 106 (C6), 11731—11742. https://doi.org/10.1029/1999JC000098

Mentaschi, L., Besio, G., Cassola, F., Mazzino, A., 2015. Performance evaluation of Wavewatch III in the Mediterranean Sea. Model, Ocean. https://doi.org/10.1016/j.ocemod.2015.04.003

Miles, J.W., 1957. On the generation of surface waves by shear flows. J. Fluid. Mech. 3 (2), 185—204. https://doi.org/10.1017/S0022112057000567

Mitsuyasu, H., Honda, T., 1982. Wind-induced growth of water waves. J. Fluid Mech. 123, 425—442. https://doi.org/10.1017/S002211208200313

Mitsuyasu, H., Maeda, Y., 2002. On the Contribution of Swell to Sea Surface Phenomena-Part 2. Int. J. Offshore Polar Eng. 12, 1053—5381.

Mitsuyasu, H., Yoshida, Y., 2005. Air-Sea Interactions under the Existence of Opposing Swell. J. Oceanogr. 61 (1), 141—154. https://doi.org/10.1007/s10872-005-0027-1

Mizuno, S., 2003. Laboratory experiments on the effects o mechanical waves on the mean and turbulent flow under the wind waves. In: Proceedings of 2003 Meeting of Japan Society of Fluid Mechanics, 41—42.

Moeini, M., Etemad-Shahidi, A., Chegini, V., Rahmani, I., 2012. Wave data assimilation using a hybrid approach in the Persian Gulf. Ocean. Dyn. 62 (5), 785—797. https://doi.org/10.1007/s10236-012-0529-5

Moon, I.J., Ginis, I., Hara, T., Tolman, H.L., Wright, C.W., Walsh, E.J., 2003. Numerical simulation of sea surface directional wave spectra under hurricane wind forcing. J. Phys. Oceanogr. 33.

Ortíz, J., Mercado, A., 2008. An intercomparison of swan and wavewatch III models with data from NDBC-NOAA buoys at oceanic scales. Coast. Eng. J. 50 (1), 47—73. https://doi.org/10.1142/S0578563408001739

Padilla-Hernandez, R., Perrie, W., Toulany, B., Smith, P., 2004. Intercomparison of Third Generation Wave Models in Shallow Water. AGU Spring Meeting Abstracts.

Peirson, W., Garcia, A., Pells, S., 2003. Water wave attenuation due to opposing wind. J. Fluid Mech. 487, 345—365. https://doi.org/10.1017/S0022112003004750

Phadke, A., Martino, C., Cheung, K.F., Houston, S., 2003. Modeling of tropical cyclone winds and waves for emergency management. Ocean Eng. 30 (4), 553—578. https://doi.org/10.1016/S0029-8018(02)00033-1

Pierson, W.J., Moskowitz, L., 1964. A proposed spectral form for fully developed wind seas based on the similarity theory of S. A. Kitaigorodskii. J. Geophys. Res. 69 (24), 5181—5190. https://doi.org/10.1029/JZ069i024p05181

Powell, M., Vickery, P., Reinhold, T., 2003. Reduced drag coefficient for high wind speeds in tropical cyclones. Nature 422 (6929), 279—283. https://doi.org/10.1038/nature01481

Rascle, N., Ardhuin, F., 2013. A global wave parameter database for geophysical applications. Part 2: Model validation with improved source term parameterization. Ocean. Model. 70, 174—188. https://doi.org/10.1016/j.ocemod.2012.12.001

Rogers, E., Babanin, A., Wang, D., 2012. Observation-Consistent Input and Whitecapping Dissipation in a Model for Wind-Generated Surface Waves: Description and Simple Calculations. J. Atmos. Oceanic Tech. 29 (9), 1329—1346. https://doi.org/10.1175/JTECH-D-11-00092.1

Rogers, W., Dykes, J., Wittmann, P., 2014. US Navy Global and Regional Wave Modeling. Oceanography 27 (3), 56—67. https://doi.org/10.5670/oceanog.2014.68

Saha, S., Moorthi, S., Pan, H.-L., Wu, X., Wang, J., Nadiga, S., Tripp, P., Kistler, R., Woollen, J., Behringer, D., 2010. The NCEP climate forecast system reanalysis. B. Am. Meteorol. Soc. 91 (8), 1015—1058. https://doi.org/10.1175/2010BAMS3001.1

Siadatmousavi, S.M., Jose, F., Miot da Silva, G., 2015. Sensitivity of a third-generation wave model to wind and boundary condition sources and model physics: A case study from the South Atlantic Ocean off Brazil coast. Comput. Geosci-UK 90 (Part B), 57—65. https://doi.org/10.1016/j.cageo.2015.09.025

Siadatmousavi, S.M., Jose, F., Stone, G.W., 2011. Evaluation of two WAM white capping parameterizations using parallel unstructured SWAN with application to the Northern Gulf of Mexico. USA. Appl. Ocean. Res. 33 (1), 23—30. https://doi.org/10.1016/j.apor.2010.12.002

Signell, R., Carniel, S., Cavaleri, L., Chiggiato, J., Doyle, J., Pullen, J., Sclavo, M., 2005. Assessment of wind quality for oceanographic modelling in semi-enclosed basins. J. Mar. Syst. 53 (1), 217—233. https://doi.org/10.1016/j.jmarsys.2004.03.006

Snyder, R.L., Dobson, F.W., Elliott, J.A., Long, R.B., 1981. Array measurements of atmospheric pressure fluctuations above surface gravity waves. J. Fluid Mech. 102, 1—59. https://doi.org/10.1017/S0022112081002528

Taylor, K.E., 2001. Summarizing multiple aspects of model performance in a single diagram. J. Geophys. Res.-Atmos. 106 (D7), 7183—7192.

Teixeira, M.A.C., Belcher, S.E., 2002. On the distortion of turbulence by a progressive surface wave. J. Fluid Mech. 458, 229—267. https://doi.org/10.1017/S0022112002007838

Thomson, J., D'Asaro, E., Cronin, M., Rogers, W., Harcourt, R., Shcherbina, A., 2013. Waves and the equilibrium range at Ocean Weather Station P. J. Geophys. Res. 118 (11), 5951—5962. https://doi.org/10.1002/2013JC008837

Tolman, H., Abdolali, A., Mickael, A., Alves, J.-H., Ardhuin, F., Babanin, A., Barbariol, F., Benetazzo, A., Bidlot, J., Booij, N., Boutin, G., Bunney, C., Campbell, T., Chalikov, D., Chawla, A., Cheng, S., Collins, C., Filipot, J.-F., Flampouris, S., Liang, Z., 2019. User manual and system documentation of WAVEWATCH III (R) version 6.07. NOAA / NWS / NCEP / MMAB Technical Note 333.

Tolman, H., Chalikov, D., 1996. Source Terms in a Third-Generation Wind Wave Model. J. Phys. Oceanogr. 26 (11), 2497—2518.

https://doi.org/10.1175/1520-0485(1996)026⟨2497:STIATG⟩2.0.CO;2

Umesh, P., Behera, M.R., 2020. Performance evaluation of input-dissipation parameterizations in WAVEWATCH III and comparison of wave hindcast with nested WAVEWATCH III-SWAN in the Indian Seas. Ocean Eng. 202, 106959. https://doi.org/10.1016/j.oceaneng.2020.106959

Young, I., 1999. Wind Generated Ocean Waves. In: Young, I.R. (Ed.), Elsevier Ocean Engineering Series. Elsevier, 1—288.

Young, I., Babanin, A., 2006. Spectral Distribution of Energy Dissipation of Wind-Generated Waves due to Dominant Wave Breaking. J. Phys. Oceanogr. 36 (3), 376—394. https://doi.org/10.1175/JPO2859.1

Young, I.R., Sobey, R.J., 1985. Measurements of the wind-wave energy flux in an opposing wind. J. Fluid Mech. 151, 427—442. https://doi.org/10.1017/S0022112085001033

Zhao, W., Guan, S., Hong, X., Li, P., Tian, J., 2011. Examination of wind-wave interaction source term in WAVEWATCH III with tropical cyclone wind forcing. Acta. Oceanol. Sin. 30 (4), 1—13. https://doi.org/10.1007/s13131-011-0128-1

Zieger, S., Babanin, A., Rogers, W., Young, I., 2011. Observation-based dissipation and input terms for WAVEWATCH III TM: implementation and simple simulations. 12th International Workshop on Wave Hindcasting and Forecasting.

Zieger, S., Babanin, A., Rogers, W., Young, I., 2015. Observation-based source terms in the third-generation wave model WAVEWATCH. Ocean Model. 96 (Pt. 1), 2—25. https://doi.org/10.1016/j.ocemod.2015.07.014